Structural Analysis Part III - X-ray tools

Session 2:

X-ray scattering and diffraction

Discovery of X-rays triggered many technological and scientific developments

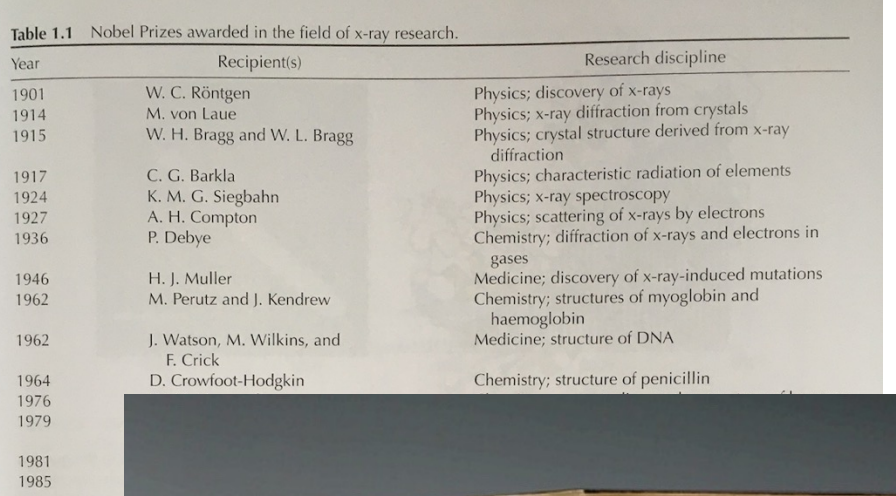




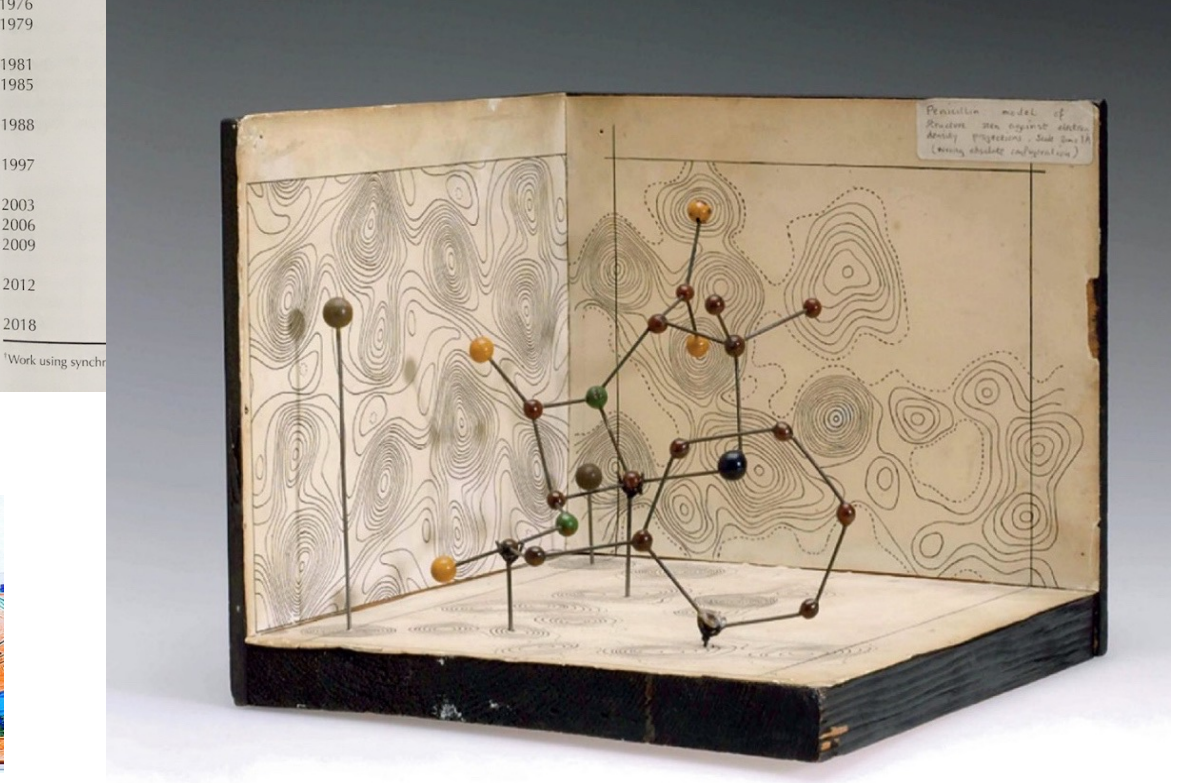


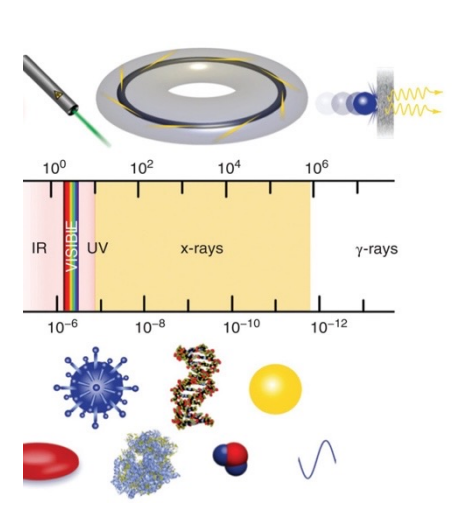












Why care about x-ray diffraction of crystals?

Why should we care about x-rays, crystals, lattices, etc?

Organic
43%

Metal-Organic
57%
At least one transition metal, lanthanide, actinide or any of Al, Ga, In, Tl, Ge, Sn, Pb, Sb, Bl, Po

Not Polymeric
89%

Single
Component
56%

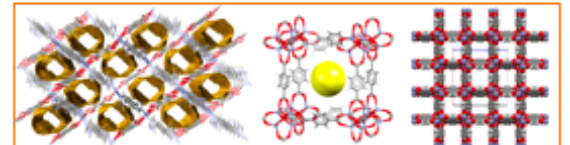
Multi
Component
44%

Organic

- Drugs
- Agrochemicals
- Pigments
- Explosives
- Protein ligands

Metal-Organic

- Metal Organic Frameworks
- Models for new catalysts
- Porous frameworks for gas storage
- Fundamental chemical bonding



Number of struct

400,000

200,000

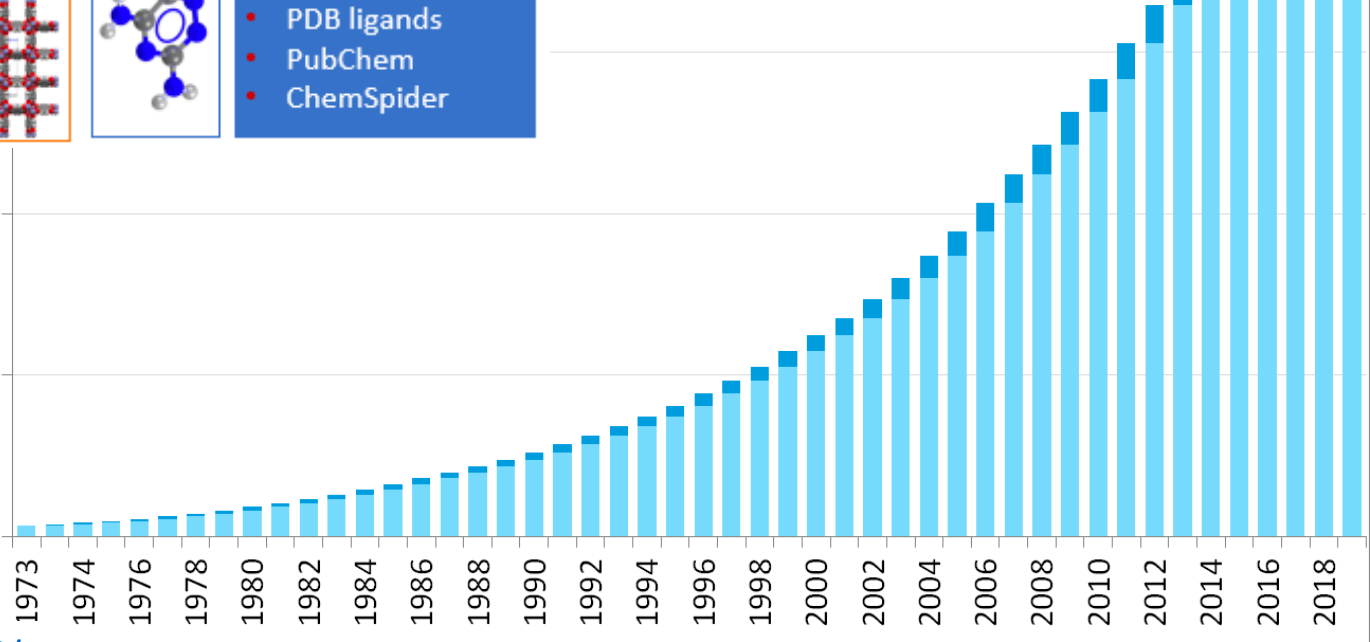
Additional data

- >10,000 polymorph families
- >160,000 melting points
- >700,000 crystal colours
- >600,000 crystal shapes
- >23,000 bioactivity details
- >9,000 natural source data
- > 250,000 oxidation states

Links and subsets

- Drugbank
- Druglike
- MOFs

Source: The Cambridge Structural Database (CSD)



Example: Diamondoids – Diamond Molecules

REPORT

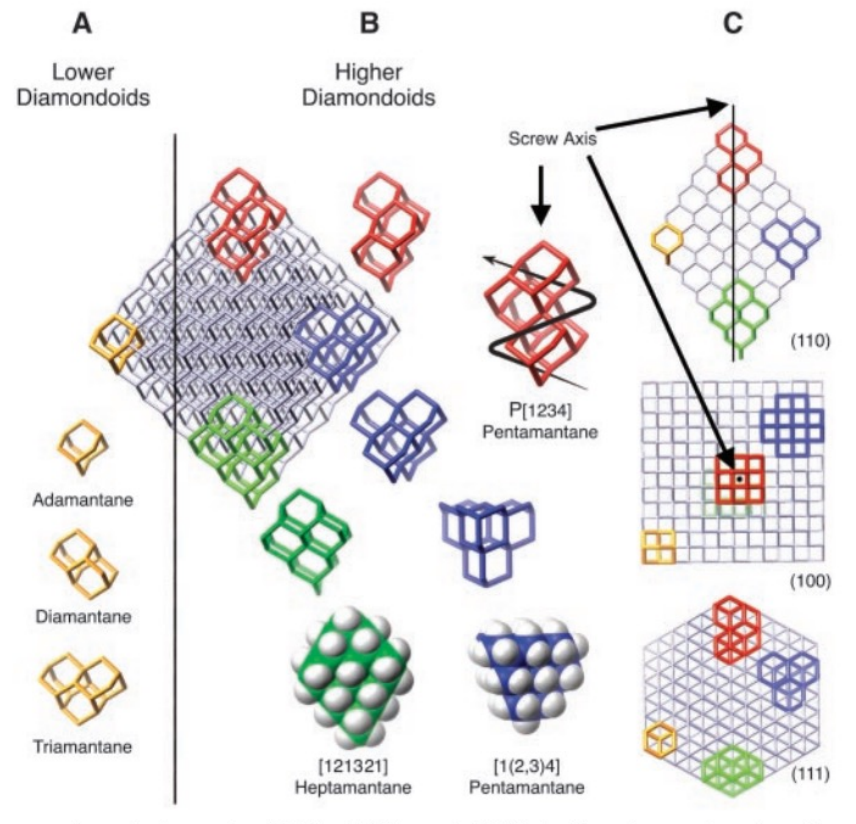
Isolation and Structure of Higher Diamondoids, Nanometer-Sized Diamond Molecules

J. E. Dahl, S. G. Liu, R. M. K. Carlson*

+ See all authors and affiliations

Science 03 Jan 2003: Vol. 299, Issue 5603, pp. 96-99 DOI: 10.1126/science.1078239

Fig. 1. The relation between the face-centered cubic diamond lattice and diamondoid structures. (A) Adamantane (yellow) is shown superimposed upon the lattice of a 455-carbon octaghedral diamond (some carbons removed for clarity). Adamantane, diamantane, and triamantane (all in yellow) are also shown separate from the diamond lattice. (B) Screwshaped higher diamondoid P [1234] pentamantane (red), pyramidal [1(2,3)4] pentamantane (blue), and rhombusshaped [121321] heptamantane (green) superimposed upon the diamond lattice and also separate from the lattice. (C) The 455-carbon diamond with superim-



posed diamondoid structures viewed along the (110), (100), and (111) lattice planes showing the diamond lattice faces of the pentamantanes and heptamantane. Views of the P [1234] pentamantane screw axis are indicated by straight arrows. The clockwise helical arrow indicates the groove in the red P [1234] pentamantane molecule.

Supplemental Material: Crystallization for XRD

Crystallization

We crystallized specific higher diamondoids from Hypercarb HPLC fractions by preparing super-saturated solutions in acetone. Crystallization vials (standard GC-MS autosampler vials) were sealed for approximately one to two weeks after which a small hole was made in the caps and the solvent allowed to evaporate. The crystals were harvested and submitted for structural determination by X-ray crystallography. Fig. S1

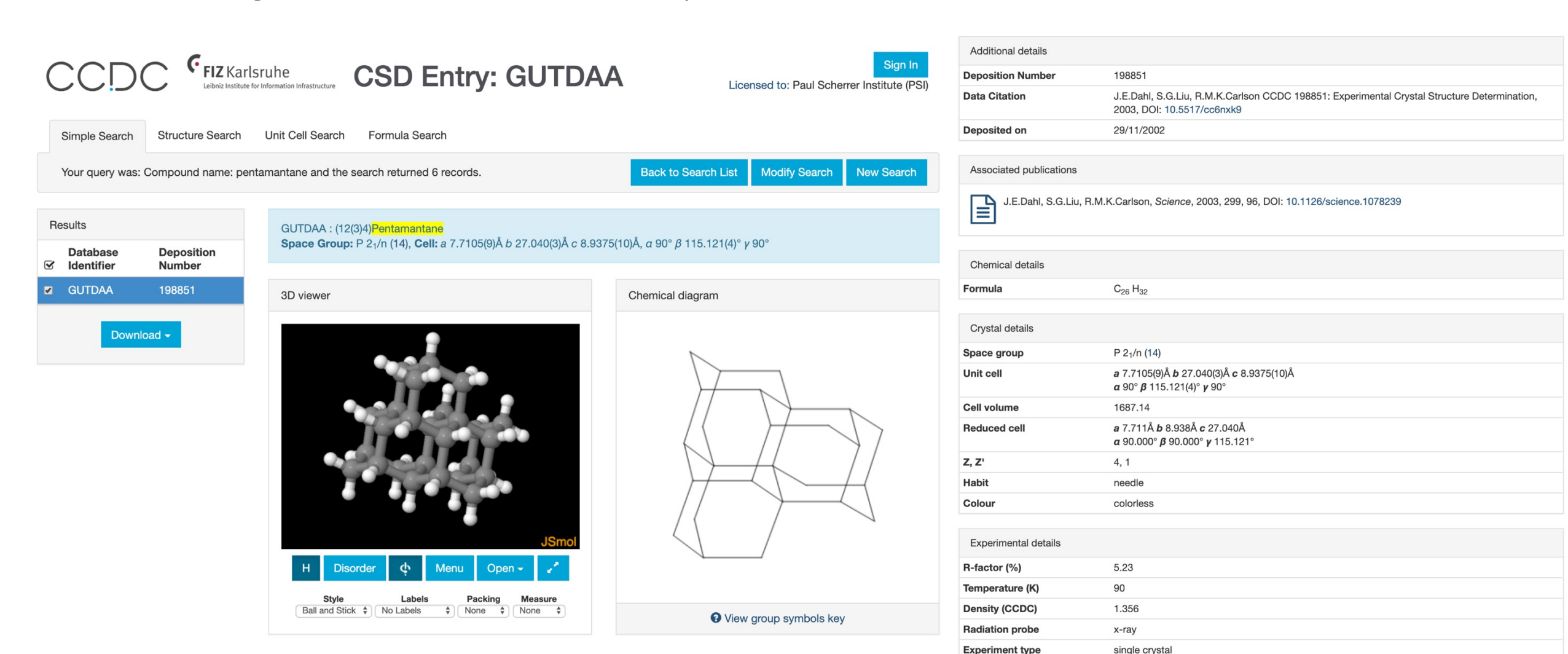
2

shows [1(2,3)4] pentamantane (structure $\underline{7}$ in Fig. 3 in the paper) grown using this method.



Fig. S1. Photomicrographs of [1(2,3)4] pentamantane crystals used for X-ray crystallography. Field of view, approx. 3.5 mm. Photograph, Marilyn Olmstead, U. C. Davis.

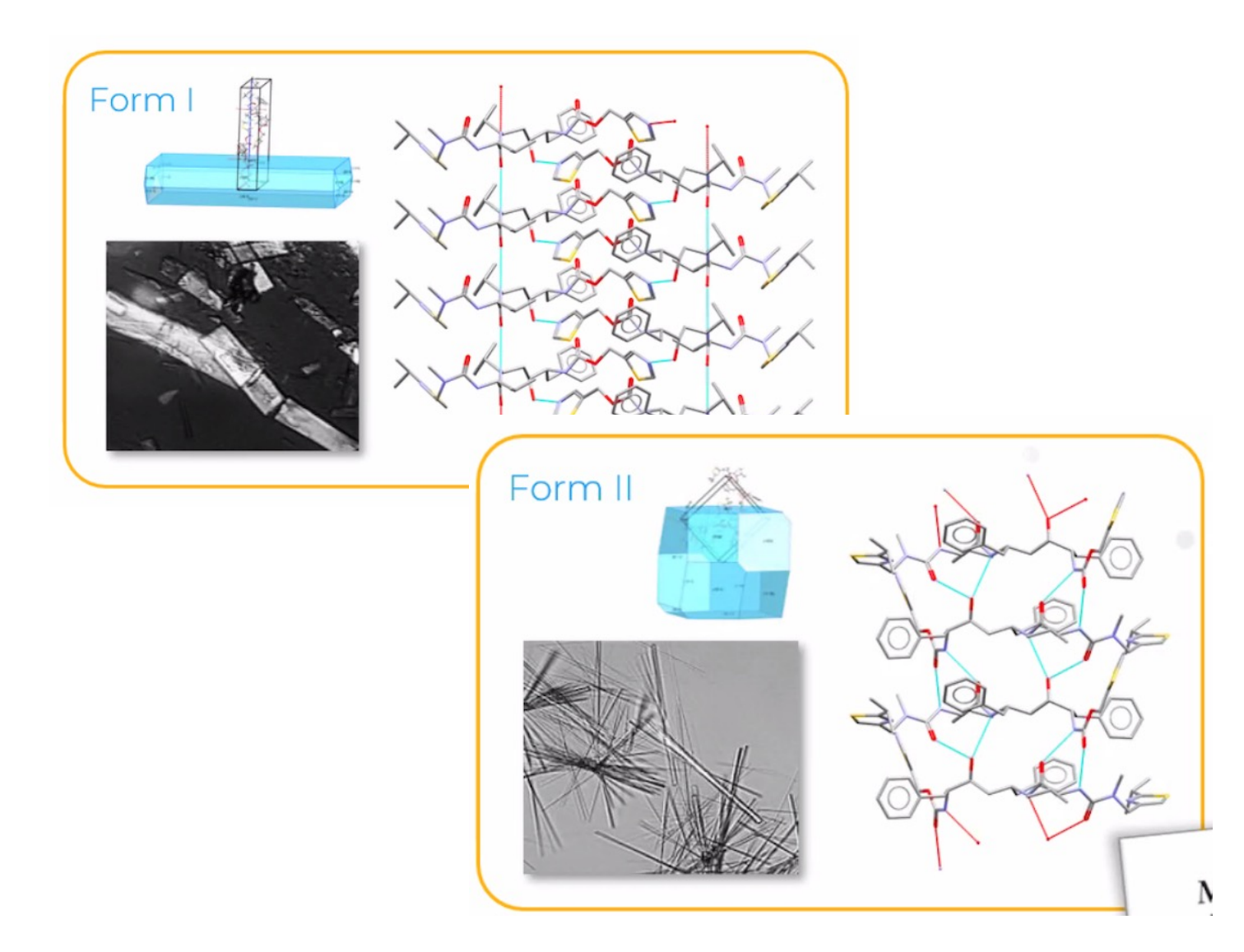
Cambridge Structural Database entry



A real world example: Crystal structure of the Novir Drug

Crystalline structure of (drug) compounds determines

- Melting properties
- Hygroscopicity
- Hydrate formation
- Soluablility
- And other properites



A real world example: Crystal structure of the Novir Drug

Science news:

> Pharm Res. 2001 Jun;18(6):859-66. doi: 10.1023/a:1011052932607.

Ritonavir: an extraordinary example of conformational polymorphism

J Bauer ¹, S Spanton, R Henry, J Quick, W Dziki, W Porter, J Morris

Affiliations + expand

PMID: 11474792 DOI: 10.1023/a:1011052932607

Abstract

Purpose: In the summer of 1998, Norvir semi-solid capsules supplies were threatened as a result of a new much less soluble crystal form of ritonavir. This report provides characterization of the two polymorphs and the structures and hydrogen bonding network for each form.

Methods: Ritonavir polymorphism was investigated using solid state spectroscopy and microscopy techniques including solid state NMR, Near Infrared Spectroscopy, powder X-ray Diffraction and Single crystal X-ray. A sensitive seed detection test was developed.

Results: Ritonavir polymorphs were thoroughly characterized and the structures determined. An unusual conformation was found for form II that results in a strong hydrogen bonding network A possible mechanism for heterogeneous nucleation of form II was investigated.

Conclusions: Ritonavir was found to exhibit conformational polymorphism with two unique crystal lattices having significantly different solubility properties. Although the polymorph (form II) corresponding to the "cis" conformation is a more stable packing arrangement, nucleation, even in the presence of form II seeds, is energetically unfavored except in highly supersaturated solutions. The coincidence of a highly supersaturated solution and a probable heterogeneous nucleation by a degradation product resulted in the sudden appearance of the more stable form II polymorph.

Similar articles

Business news:



Abbott Reports Production Problems For Norvir

27-07-1998

Abbott Laboratories has reported that it is having difficultiesmaintaining production of its HIV protease inhibitor Norvir (ritonavir). The problems are related to its capsule formulation of the antiretroviral.

"We have encountered an undesired formation of a Norvir crystalline structure that affects how the capsule form of Norvir dissolves," commented Arthur Higgins, senior vice president for pharmaceutical operations at Abbott. Although the problem has been identified, to date the company has been unable to come up with a solution.

Abbott stressed that capsules already in circulation are not affected, but there will be shortages and an interruption in supply of the product. Given the seriousness of interrupting treatment in highly-active antiretroviral therapy (which could be associated with the development of resistance and ultimately treatment failure), Abbott is planning to manufacture Norvir in a substitute oral solution so that patients on the drug can maintain their supply. It is estimated that 60,000-70,000 people with HIV are taking the drug.

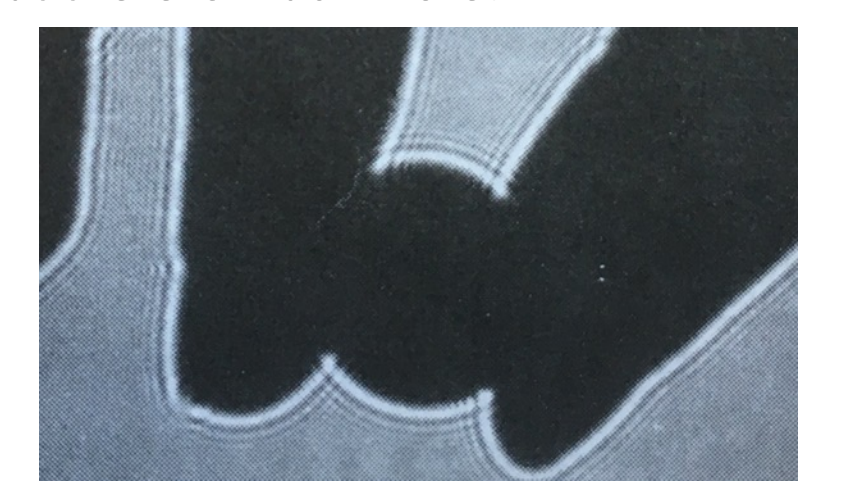
Effect On Full-Year Sales? Abbott had been projecting sales of around \$250 million for Norvir in 1998, and as yet it is unclear whether the supply problems will impact this figure. Sales of the drug last year were around \$170 million, less than the performance seen with the other protease inhibitors in 1997. Datamonitor says that Merck & Co's Crixivan (indinavir) had sales of \$240 million last year, while Agouron's Viracept (nelfinavir) made around \$190 million last year, and Roche's Invirase (saquinavir) made over \$200 million.

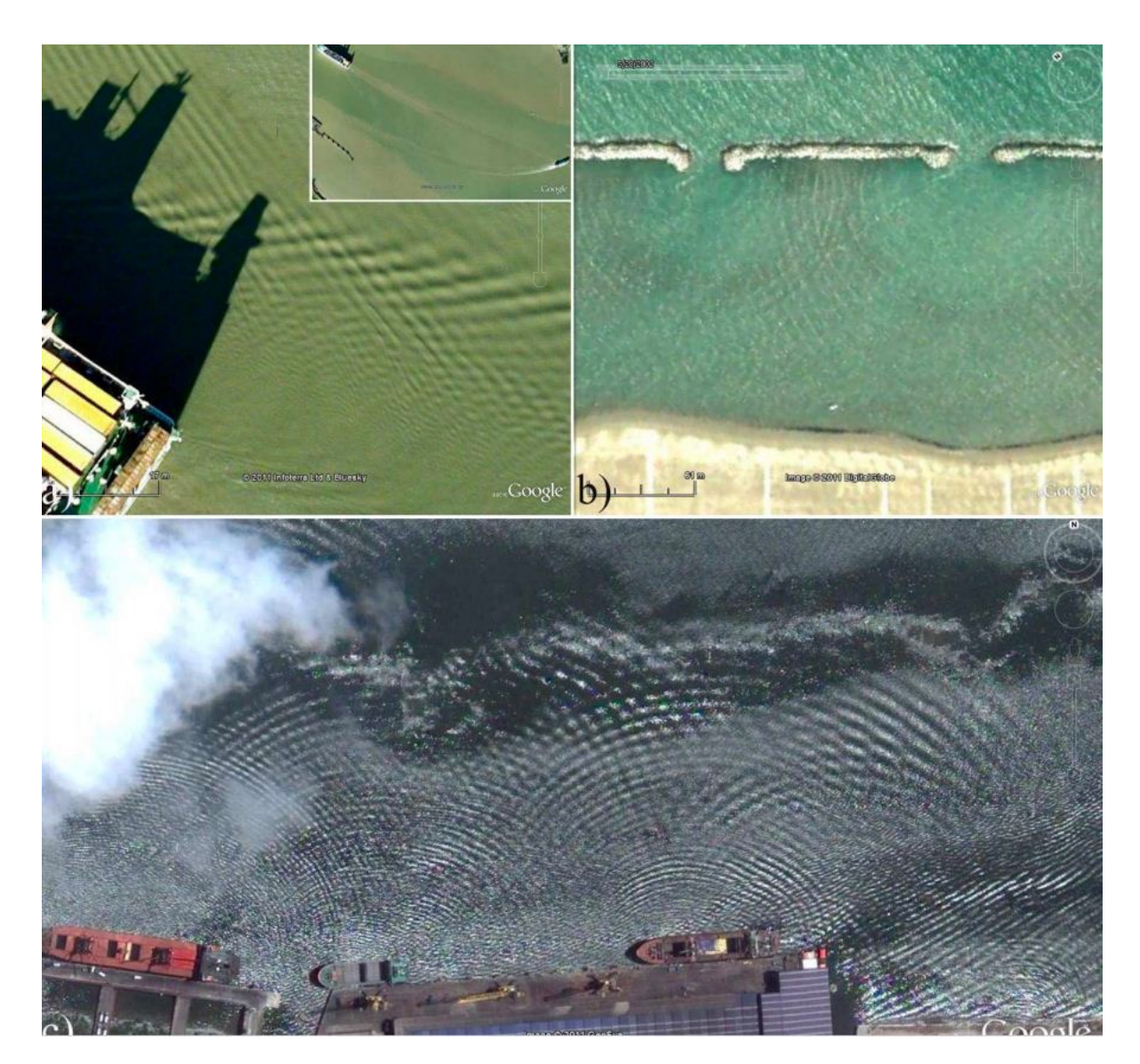
Analyst Hemant Shah of HKS & Co told Reuters that the other protease inhibitors would definitely gain market share at the expense of Norvir, adding that the impact on Abbott's bottom line will depend greatly on the duration of the problem.

Some very basics about diffraction and scattering

Diffraction, a short review

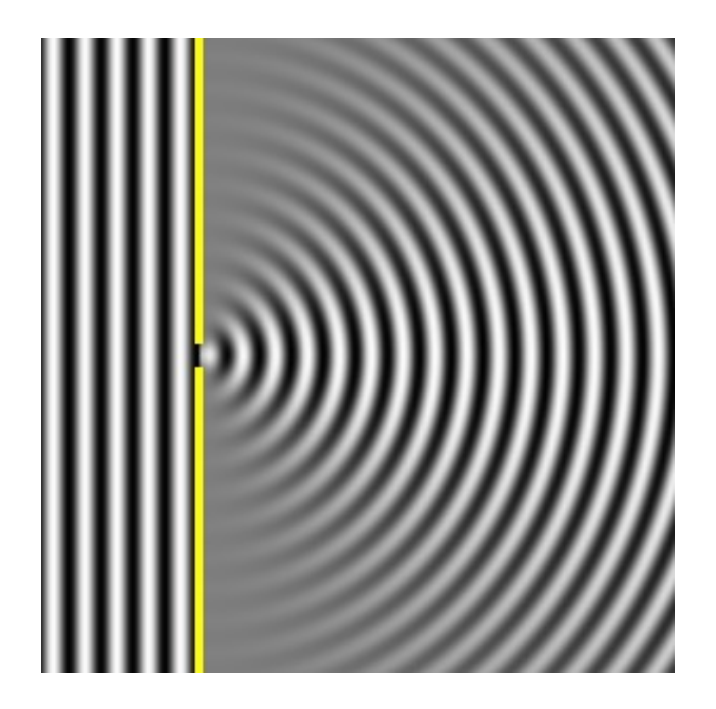
- Should be familiar concept
- A wave encountering an object changes its wavefront. Note that this can also be a density change (later more)
- Fundamental properties of all waves with relevant effects from electron microscopy to shaping coastal landscapes
- In optics most commonly known for limiting resolution in optical setups (microscopes)
- But there is much more!





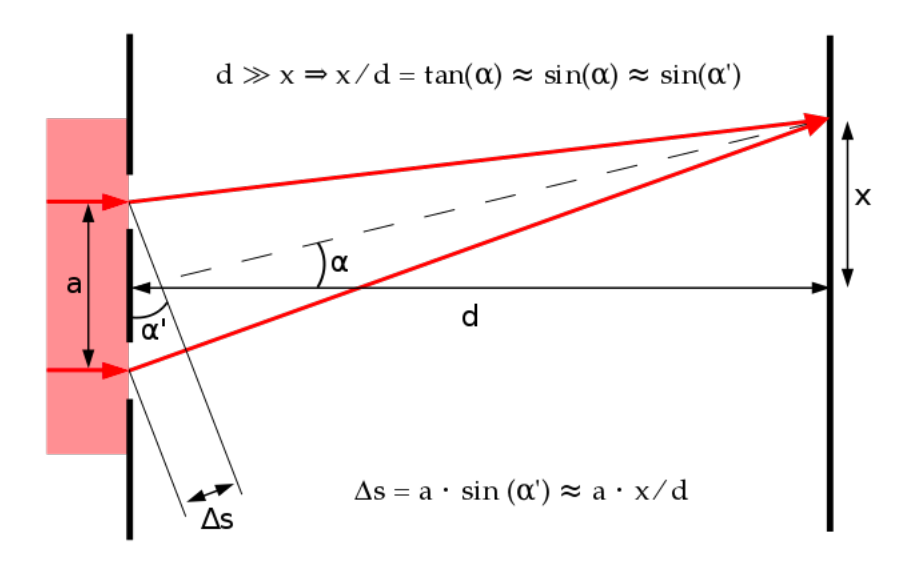
The Huygens-Fresnel Principle

- Hugens: every point a wave (a luminous disturbance) reaches becomes a source of a spherical wave; the sum of these secondary waves determines the form of the wave at any subsequent time.
- Huygens-Fresnel: every unobstructed point of a wavefront serves as a source of spherical secondary wavelets. The amplitude of the wave beyond is the superposition of all these wavelets. (includes amplitude and relative phase)



Diffraction from a single slit

The double slit



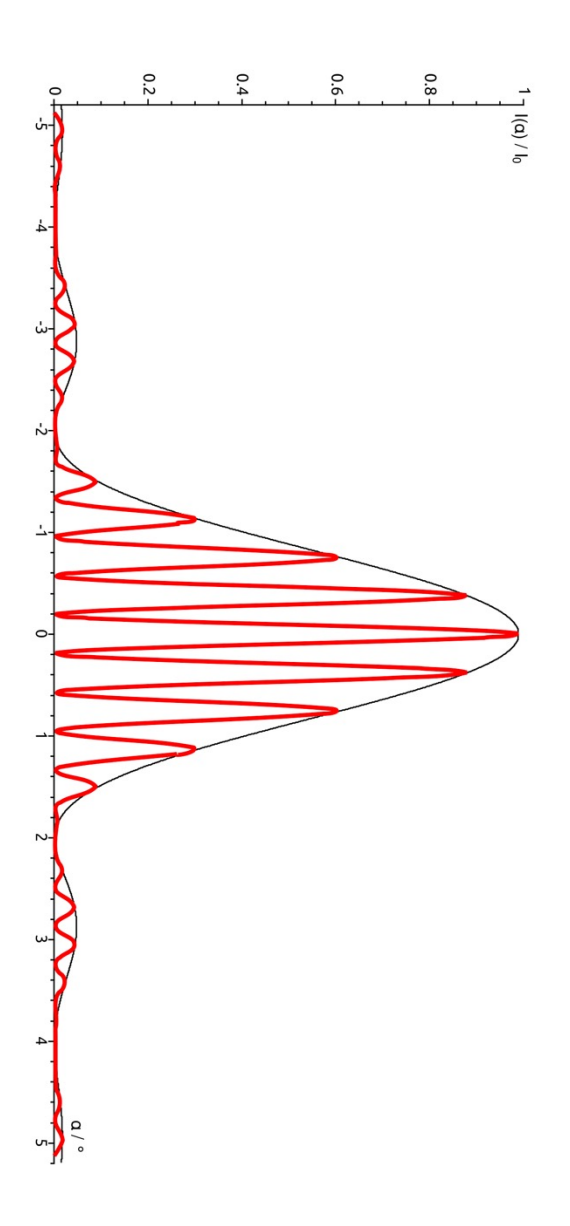
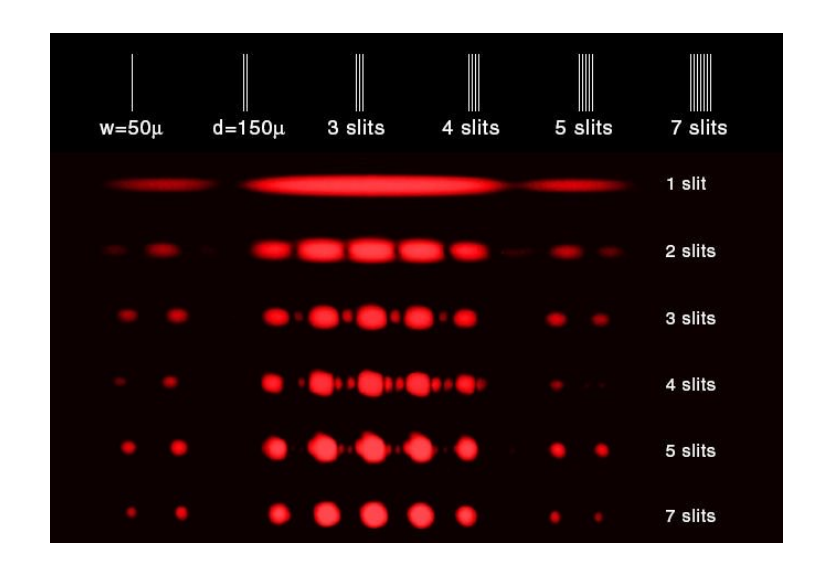
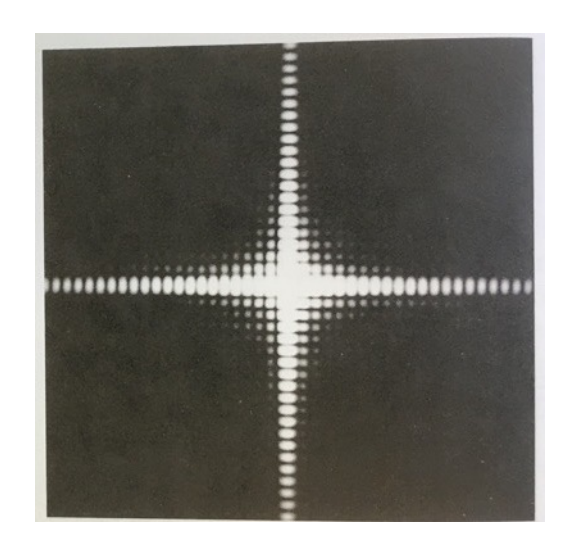
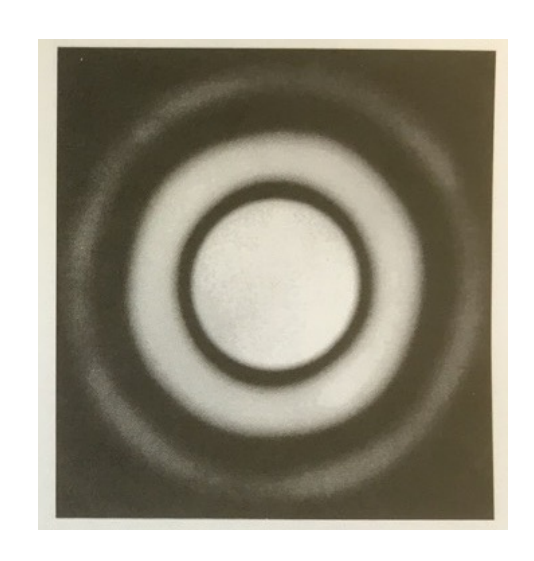


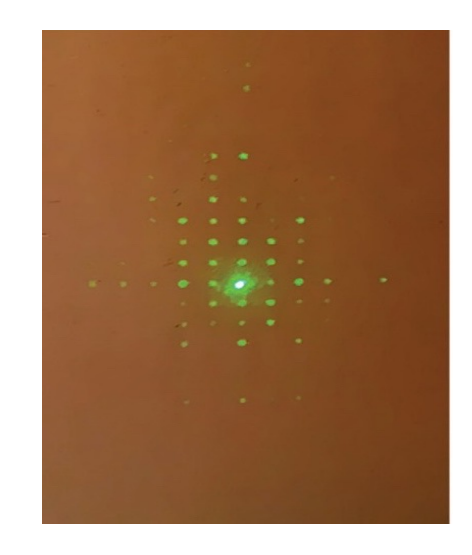
Image source: wikipedia

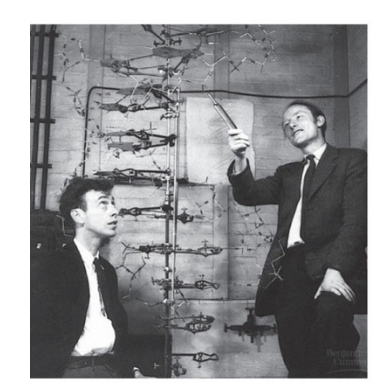
Diffraction examples



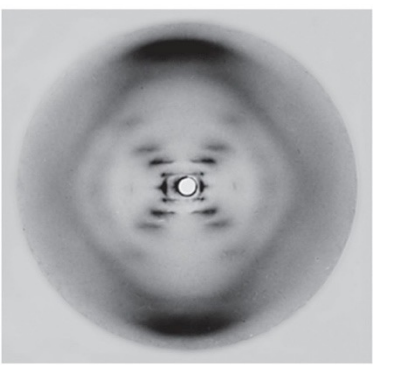




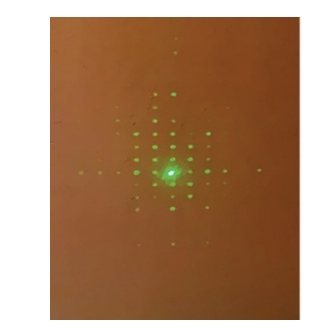


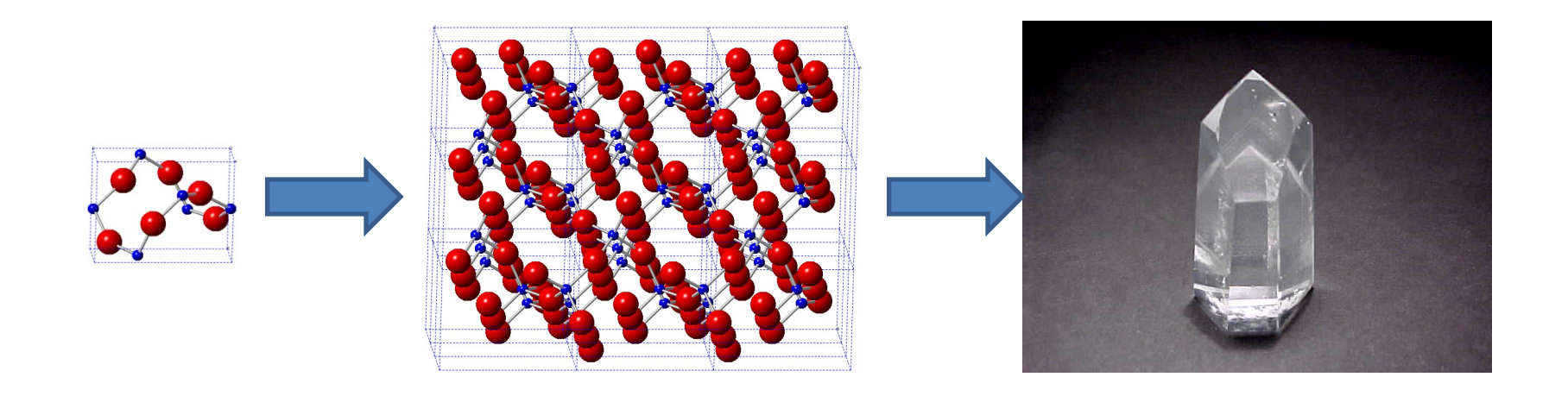


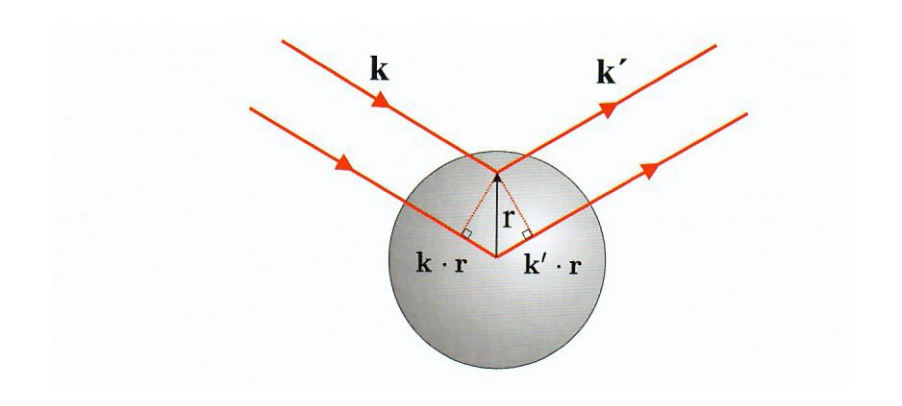


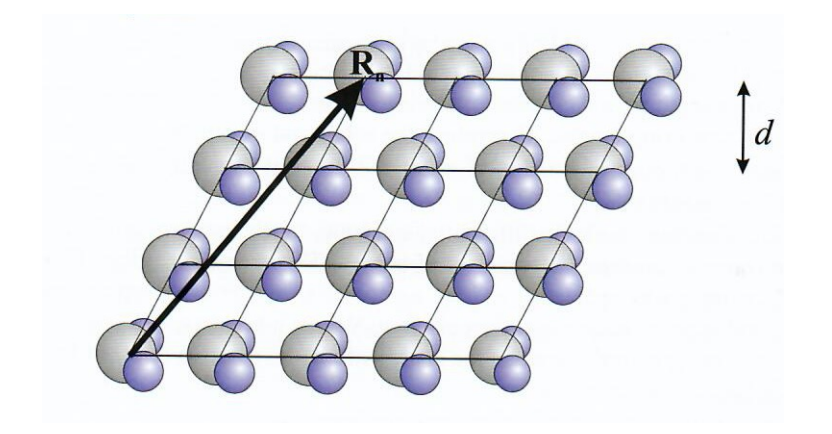


Crystaline materials are characterized by the long-range order

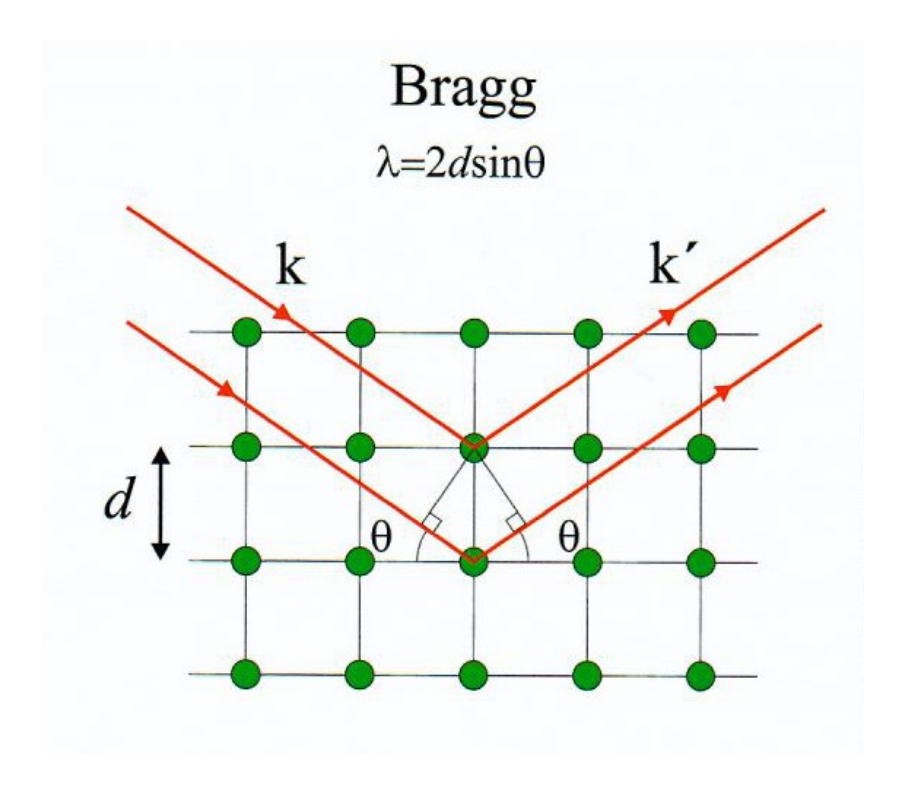


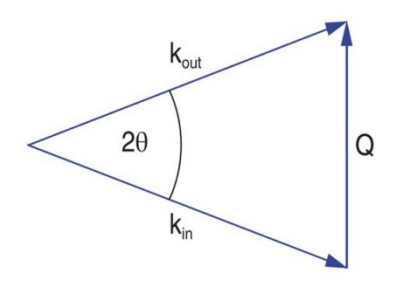






Bragg scattering





The Nobel Prize in Physics 1915

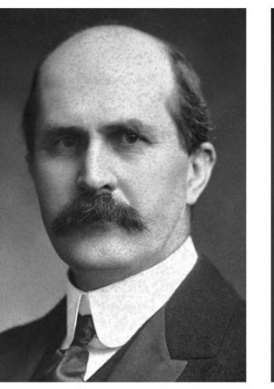


Photo from the Nobel Foundation archive.

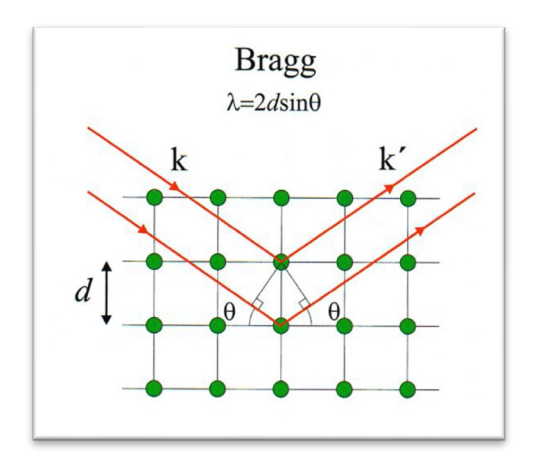
Sir William Henry Bragg Prize share: 1/2

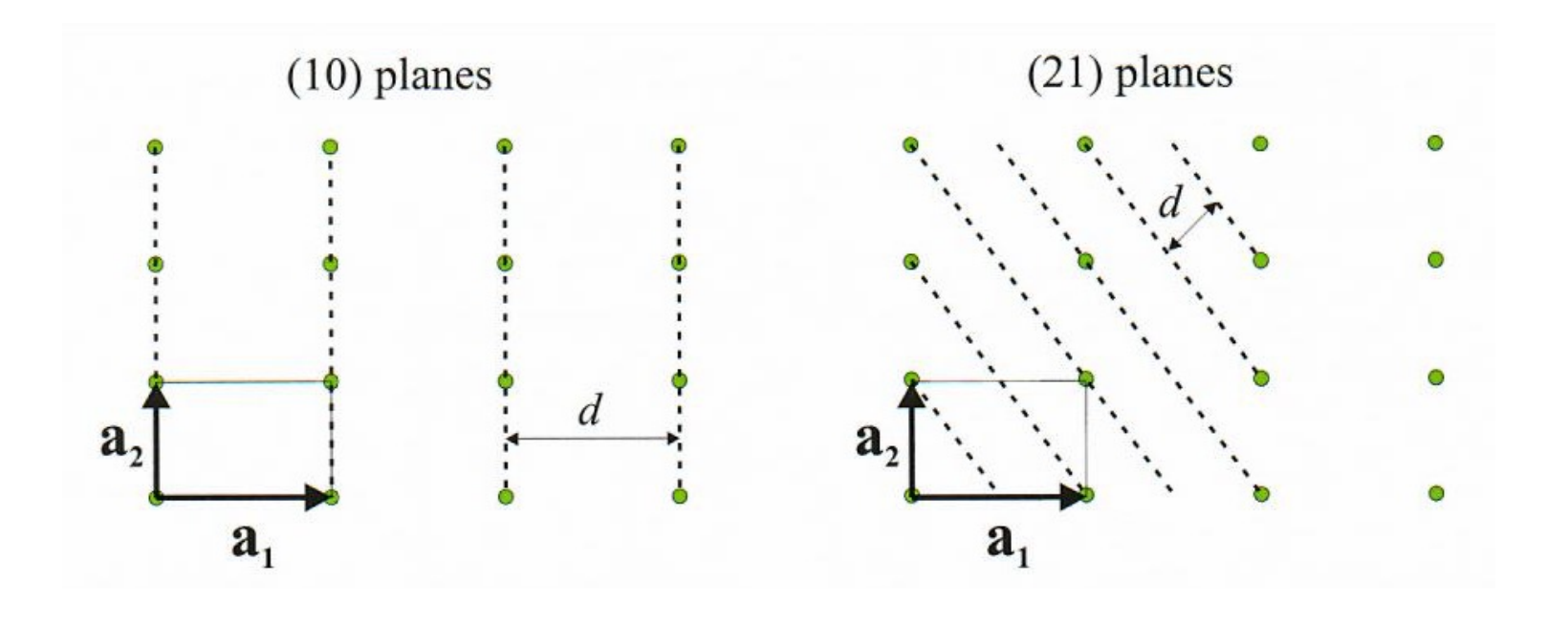
Photo from the Nobel Foundation archive.

William Lawrence Bragg

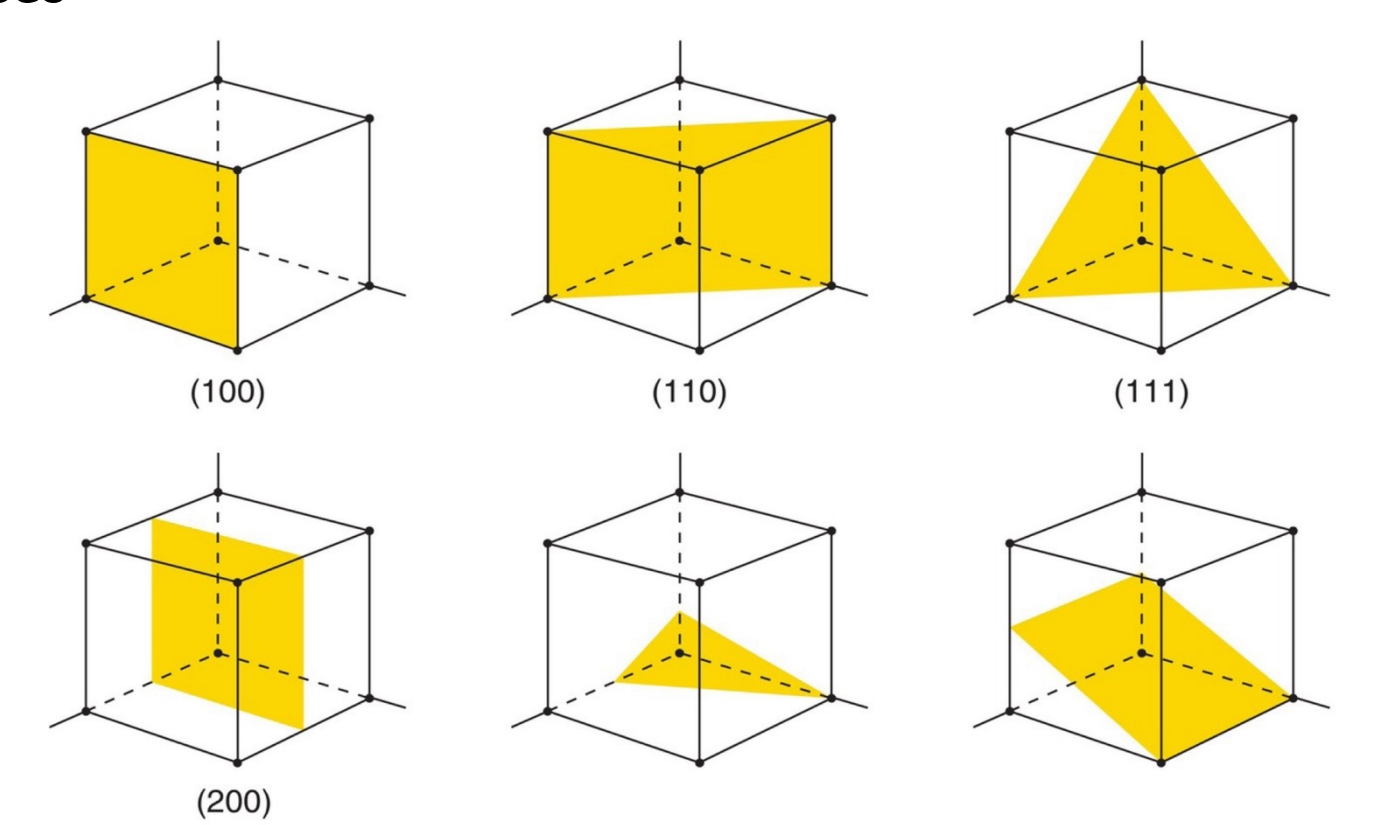
Prize share: 1/2

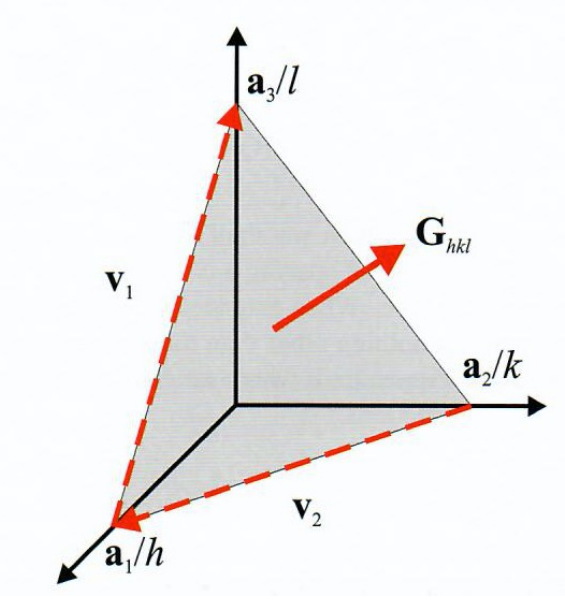
Lattice planes



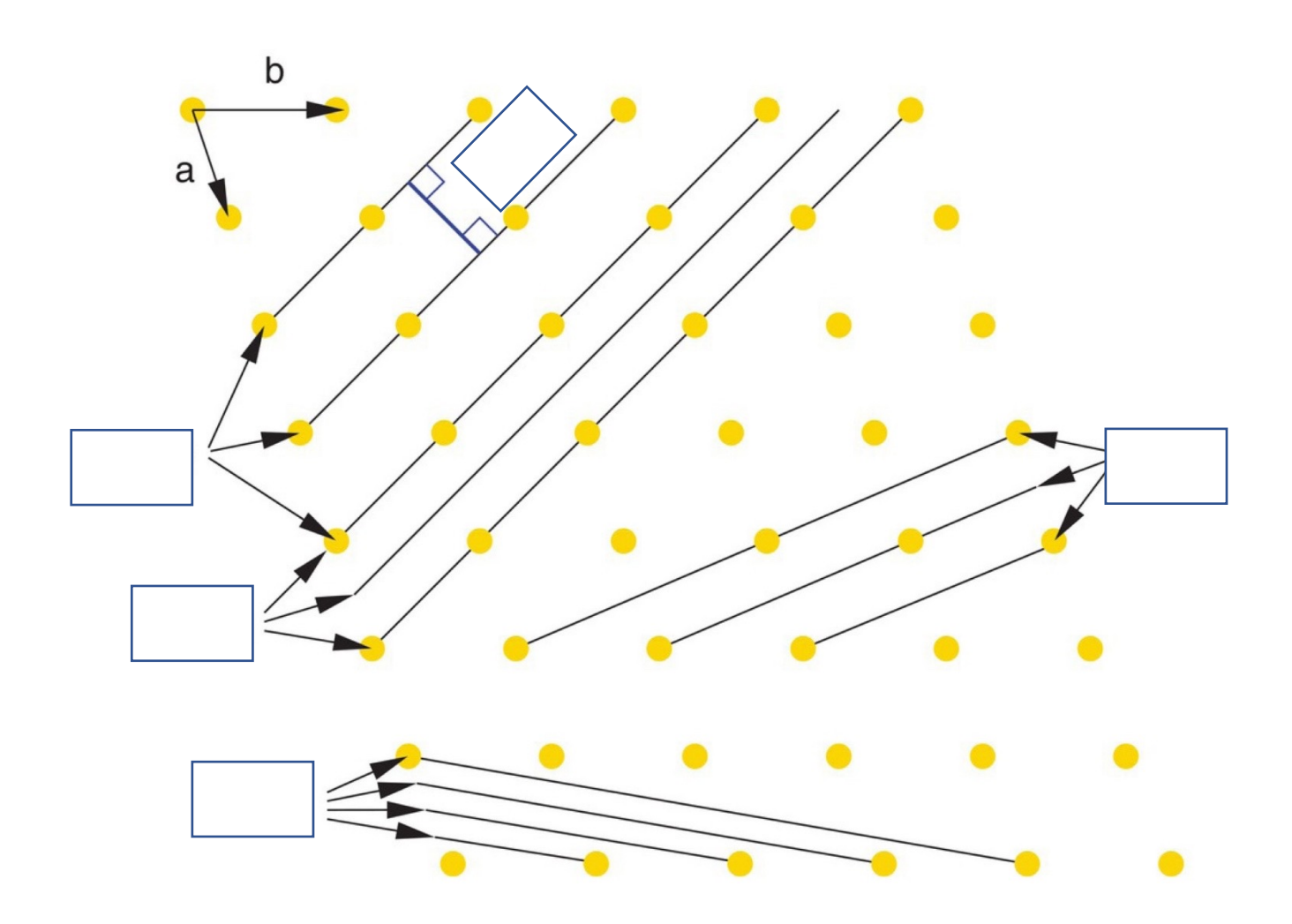


Miller indices

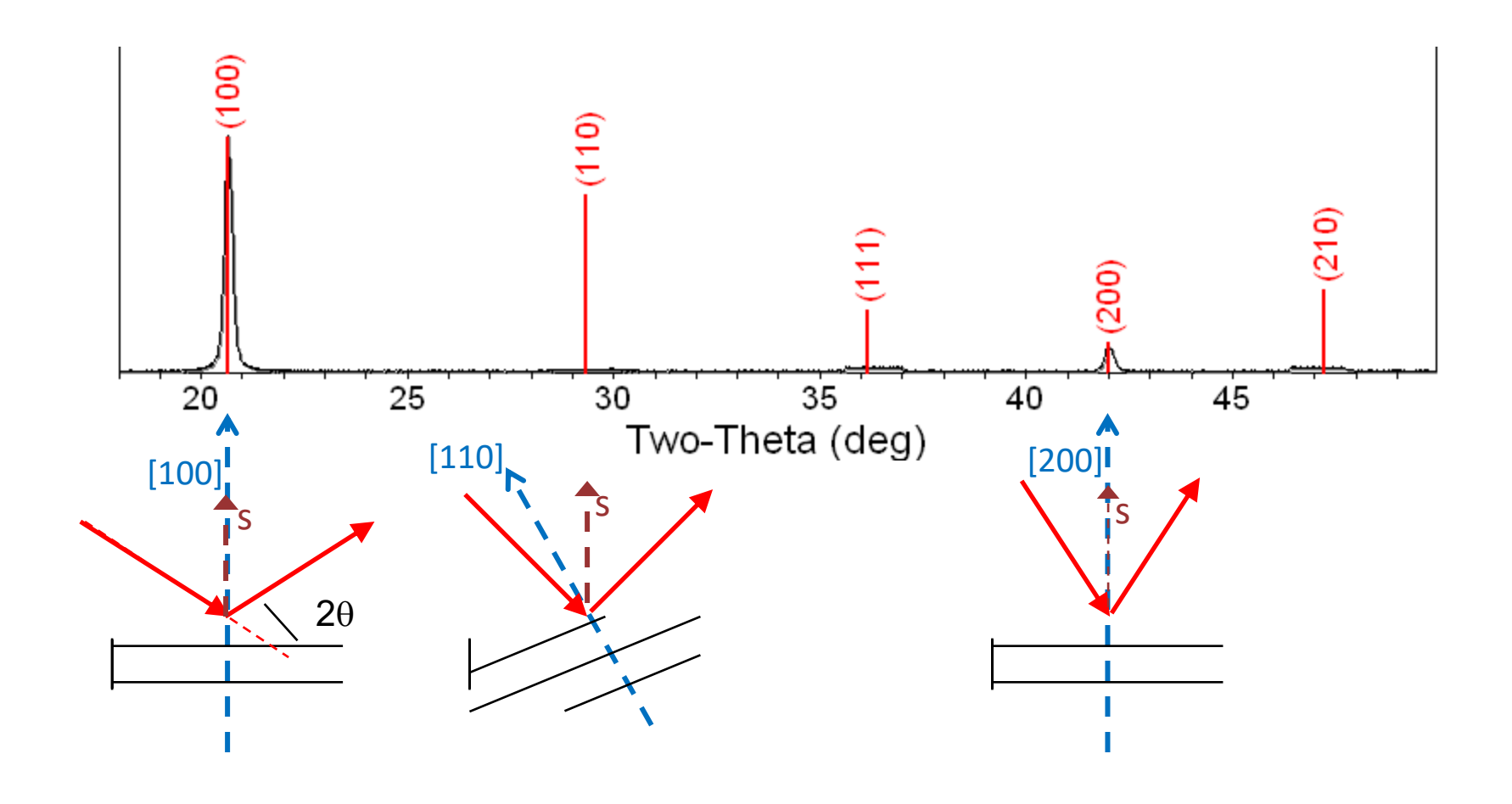




Exercise: Identify lattice planes

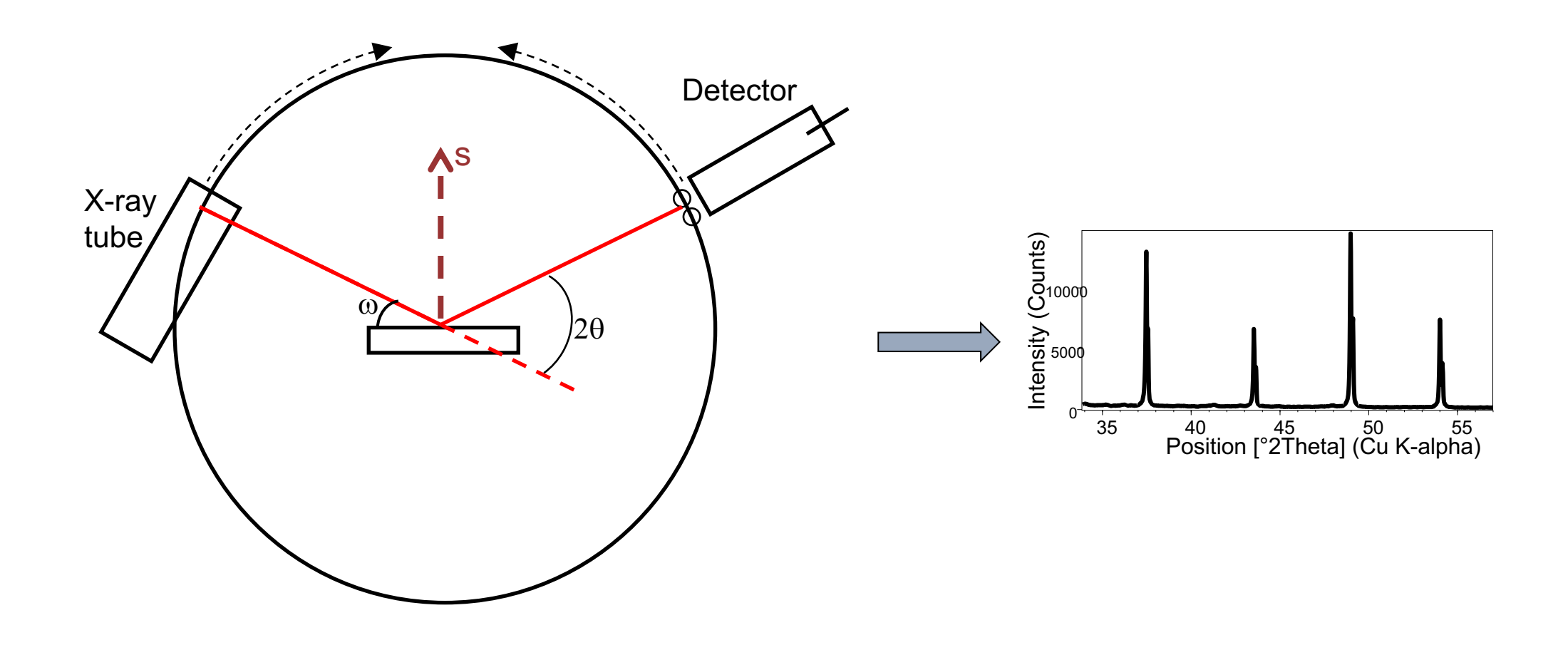


A single crystal (typically) produces one family of Bragg peaks for fixed geometry and λ

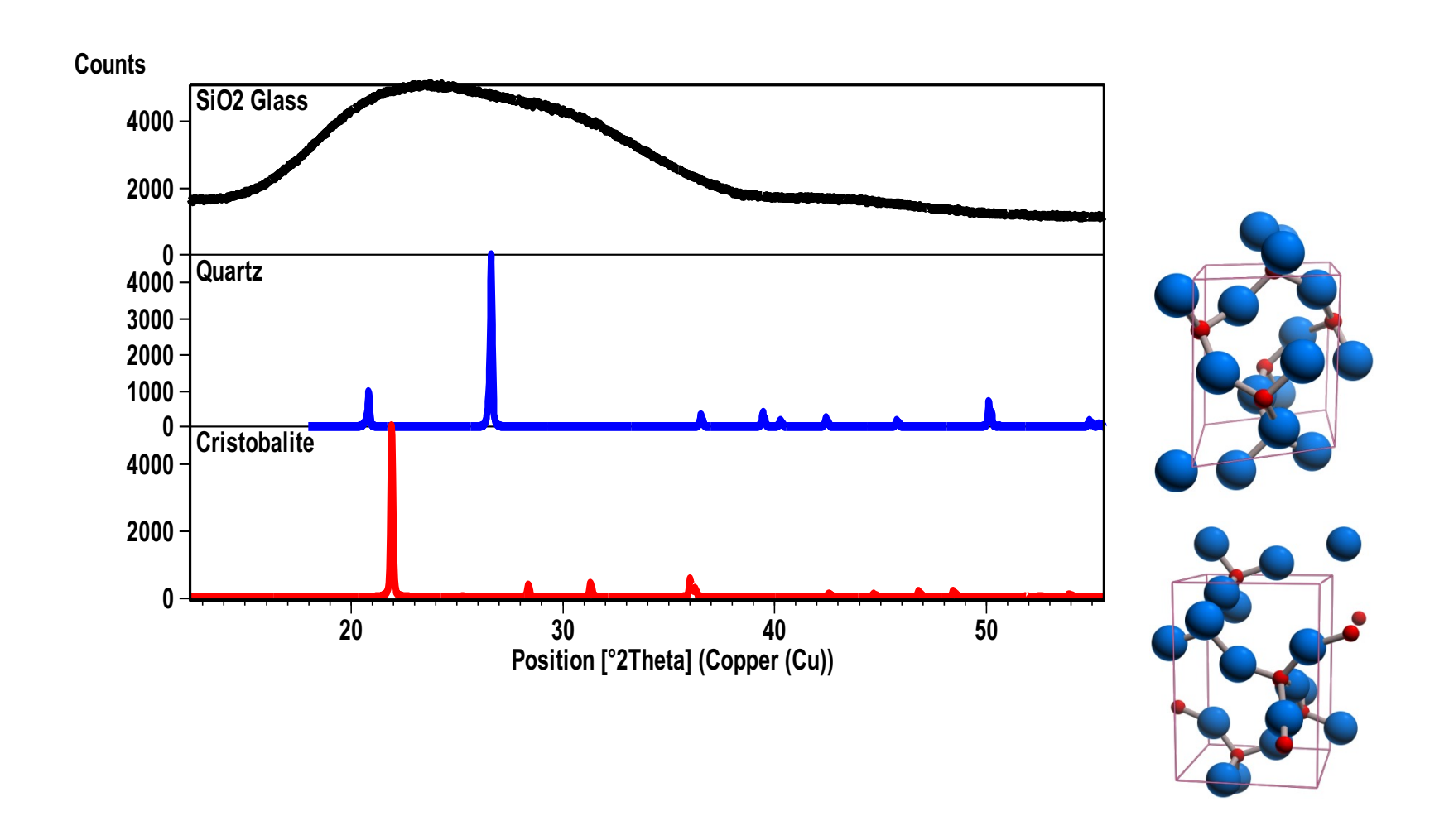


Diffraction examples

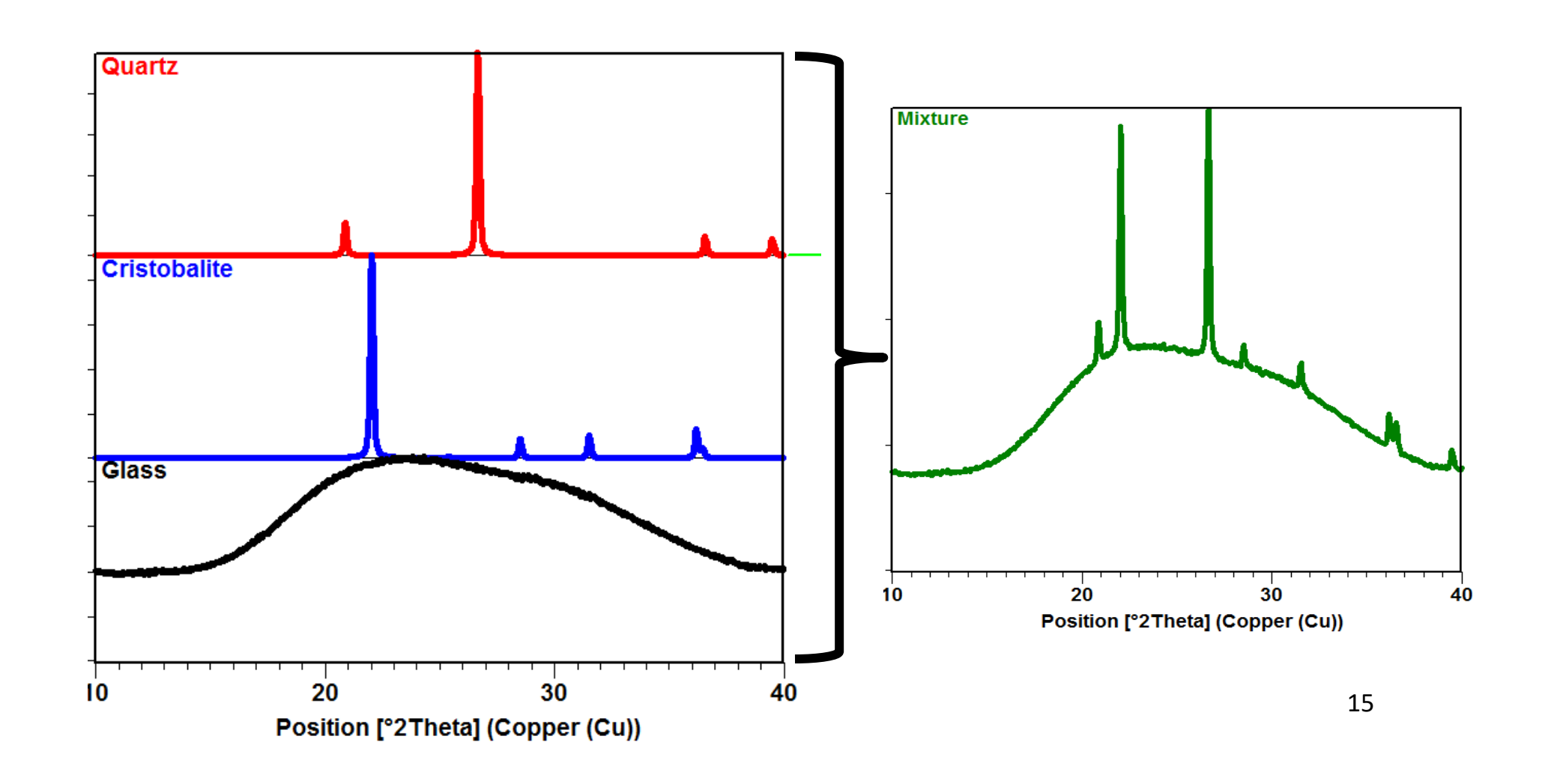
Diffraction experiment - example



Characteristic signals from different – chemically identical – samples

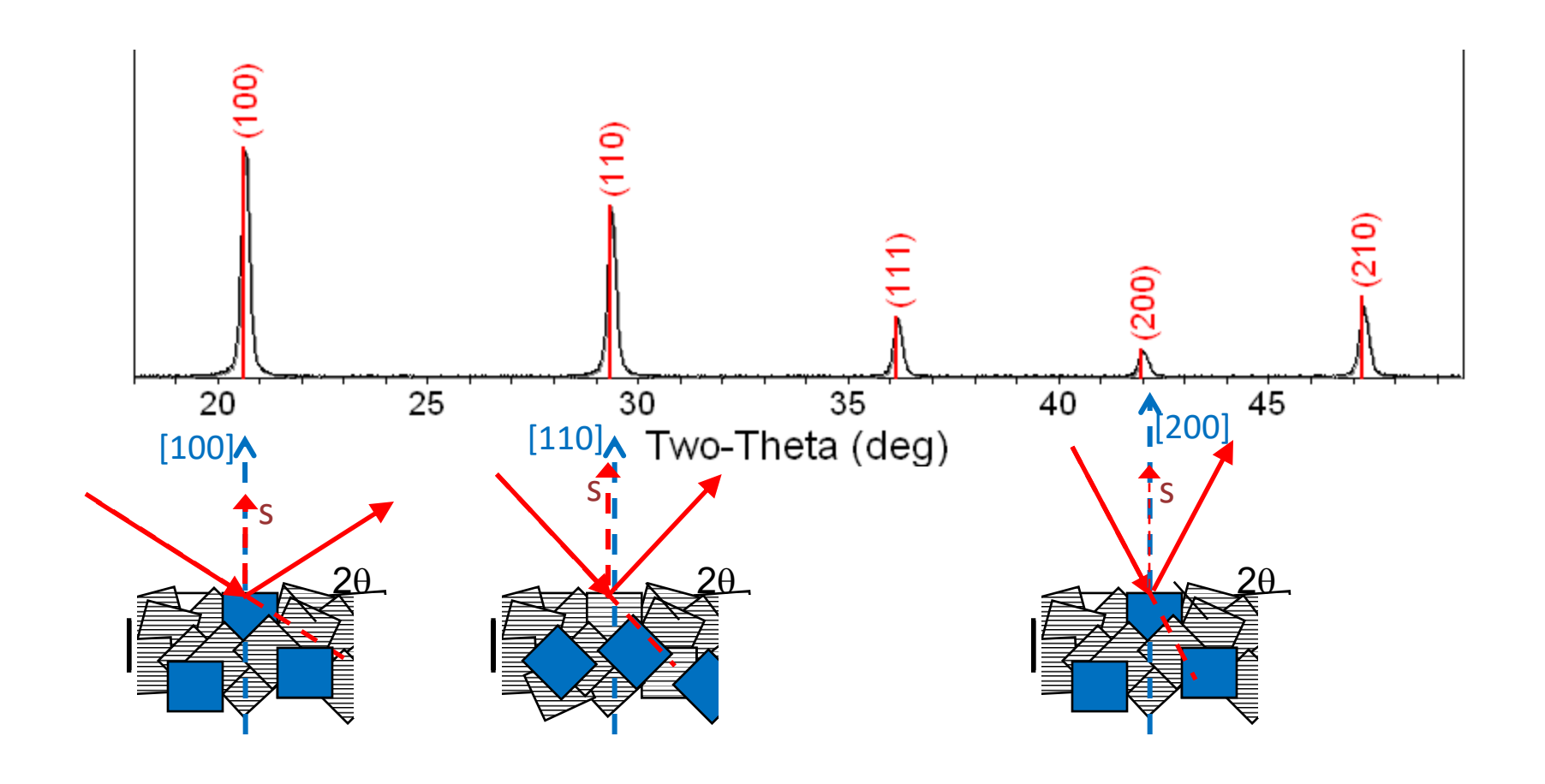


The diffraction pattern of a mixture is a simple sum from each component phase

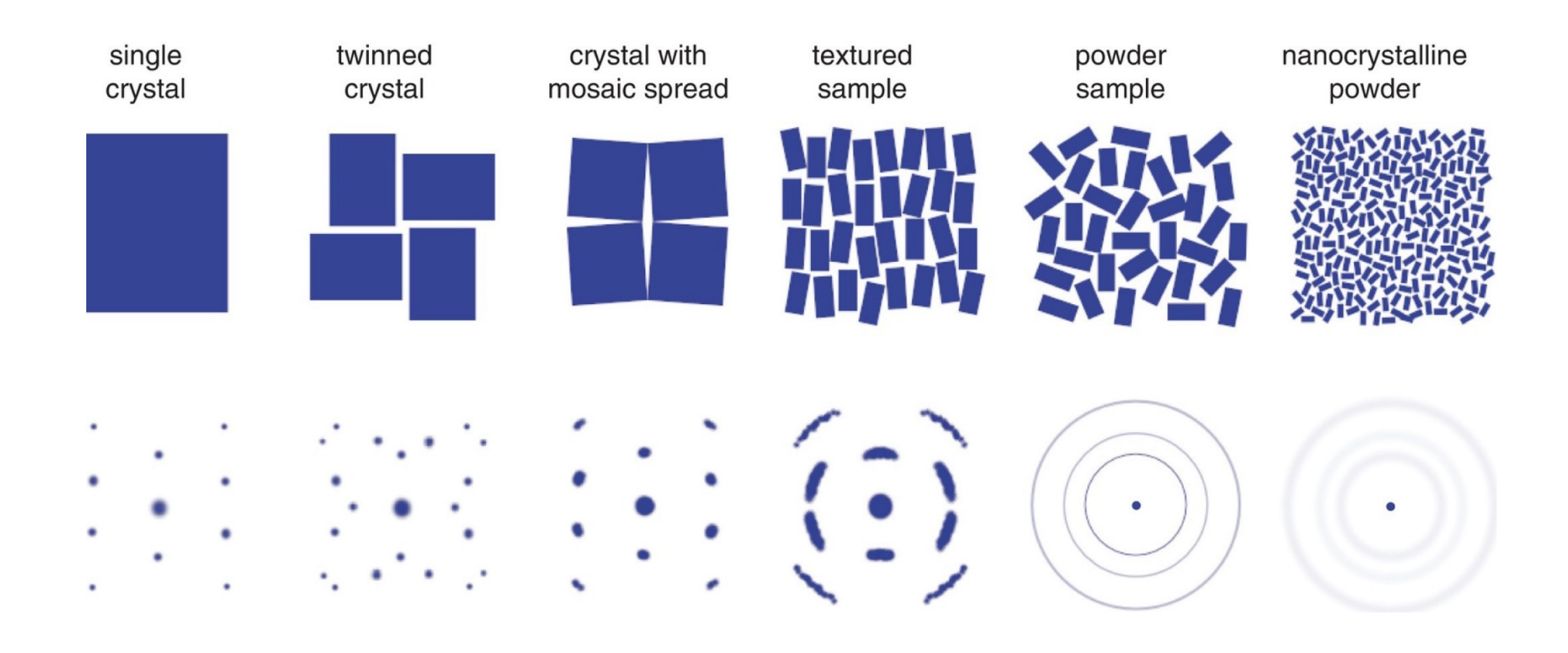


Powder diffraction

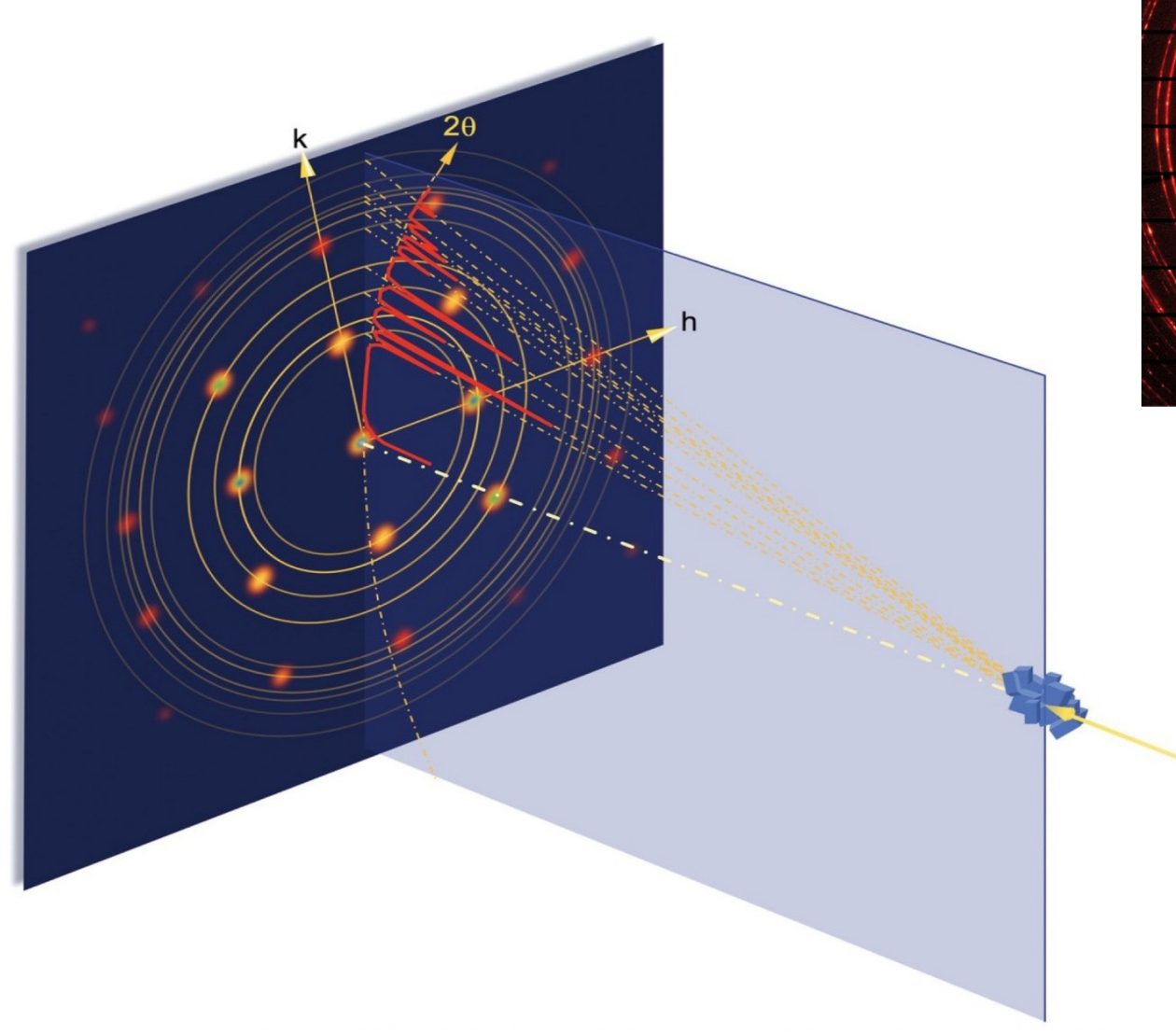
Diffraction of a polycrystalline sample

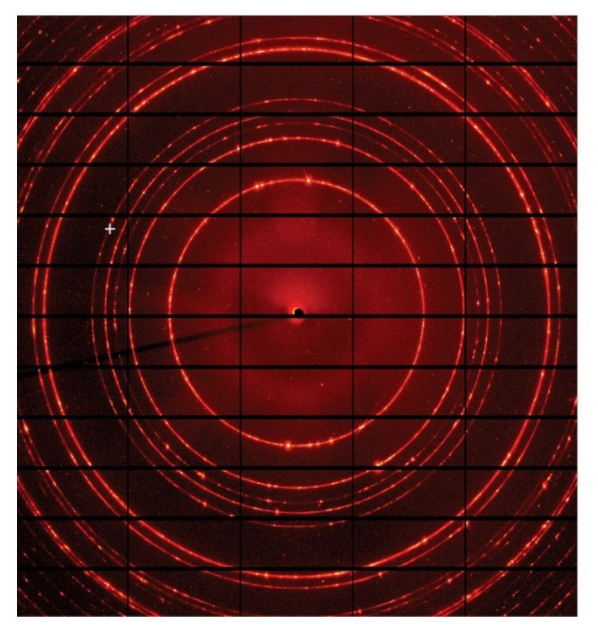


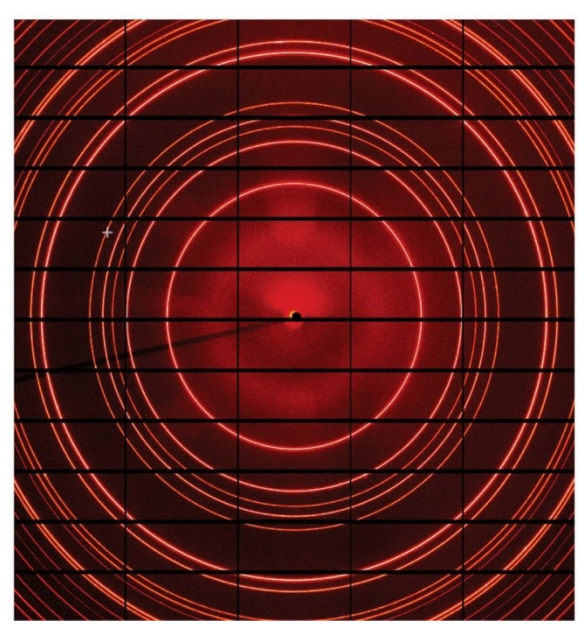
Diffraction signal of different sample types



Powder diffraction experiments







Powder diffraction geometry

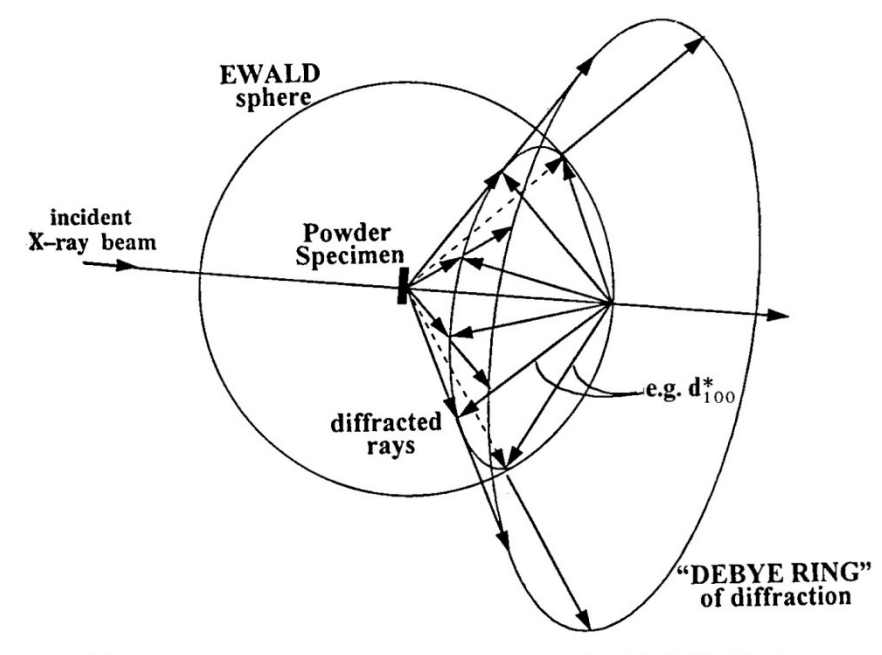
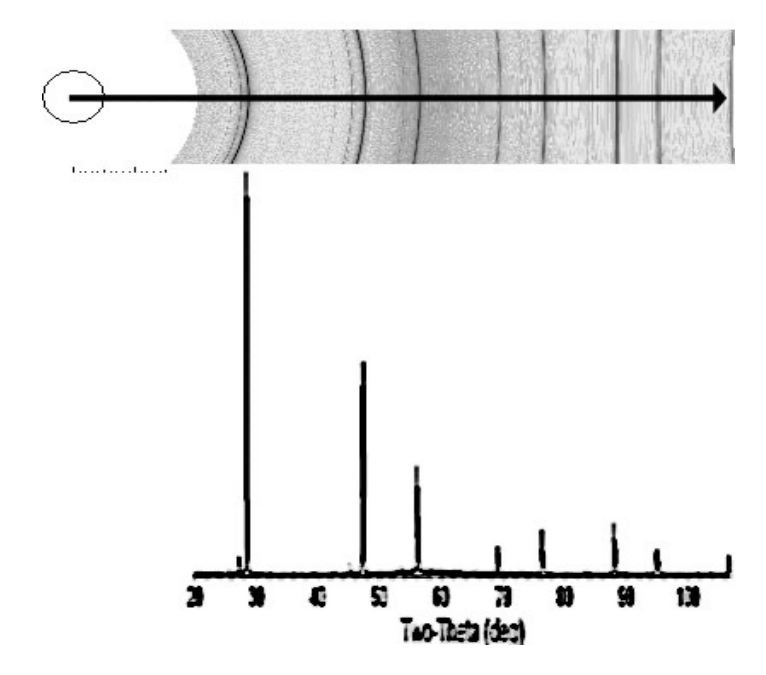
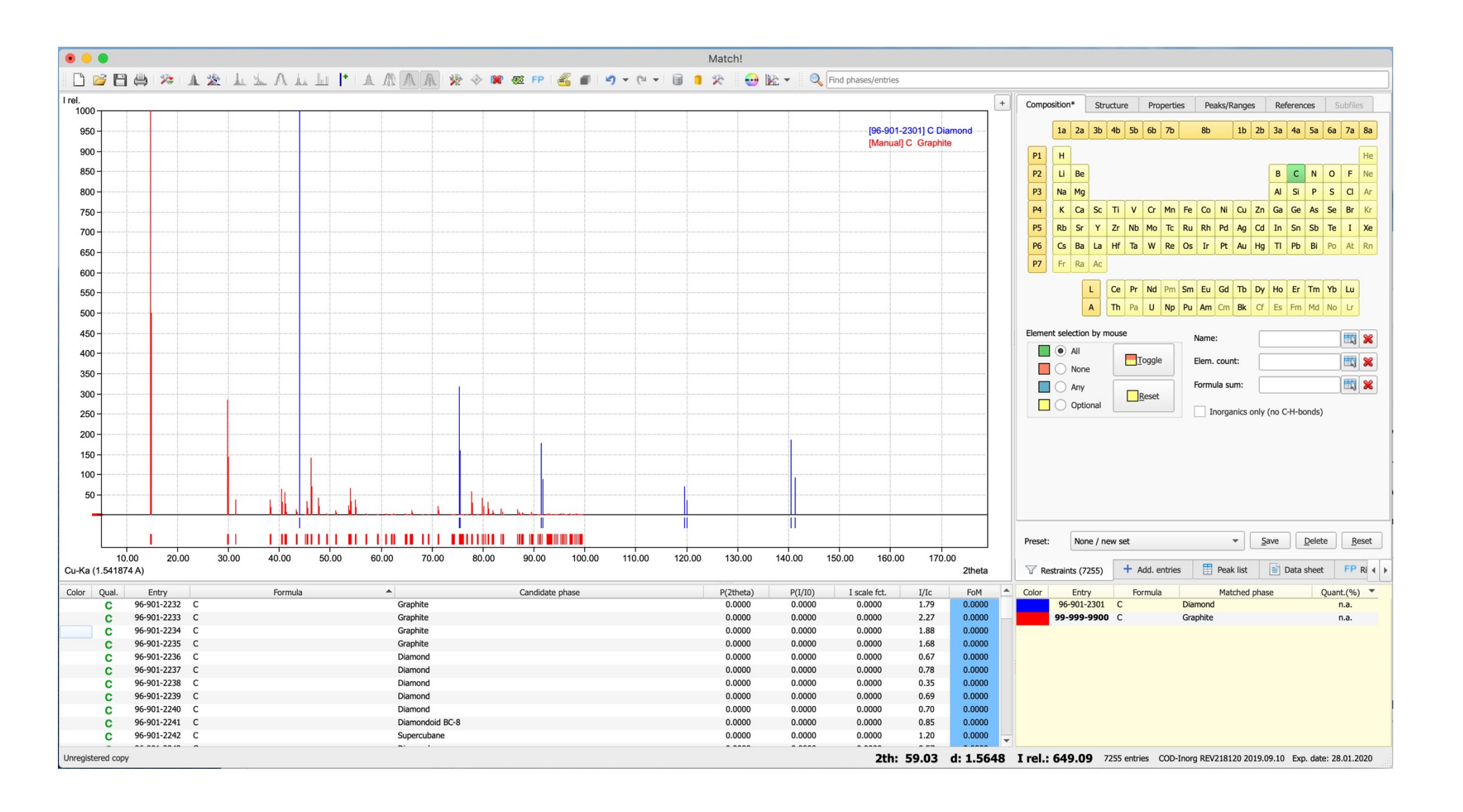


Figure 3.9. The intersection of \mathbf{d}_{100}^* vectors from a powder with the Ewald sphere.

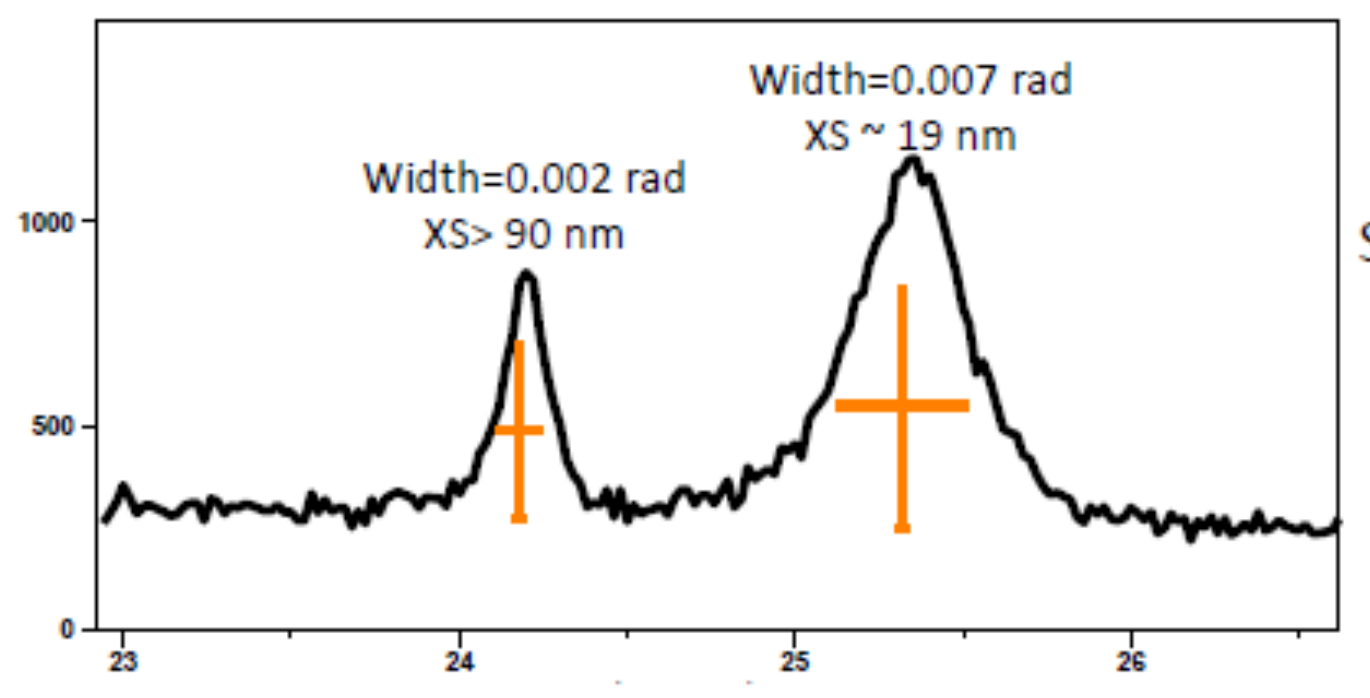


Powder diffraction data bases for elemental analysis

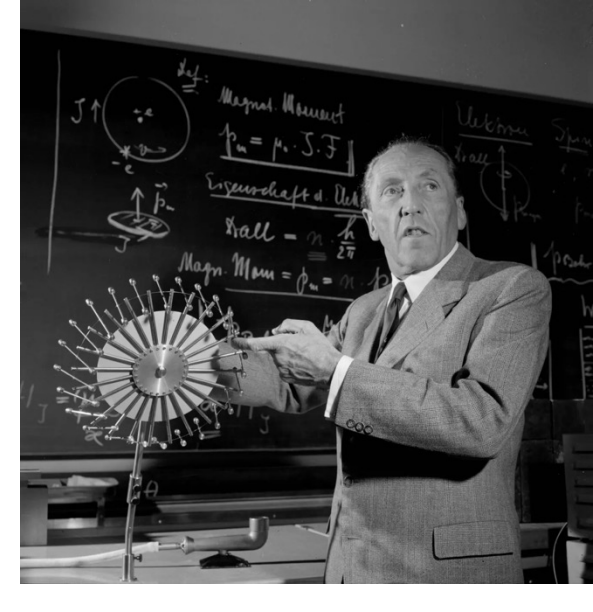


Debye-Scherrer Formula

The diffraction peak width may contain microstructural information



$$Size = \frac{K\lambda}{Width*\cos\theta}$$



Paul Scherrer Swiss Physicist (1890-1969)

Exercise: Colloidal nanoparticles

The diffraction experiments were carried out with a Stoe STADI-P X-ray powder diffractometer at University College London with a Ge(111) monochromator before the sample. A Cu $K\alpha_1$ X-ray beam of wavelength 0.154056 nm was used. The samples were measured in 0.35 mm diameter glass capillaries at room temperature. Capillary diameters were checked to be equal with a micrometer. The diffraction patterns were collected using a position-sensitive

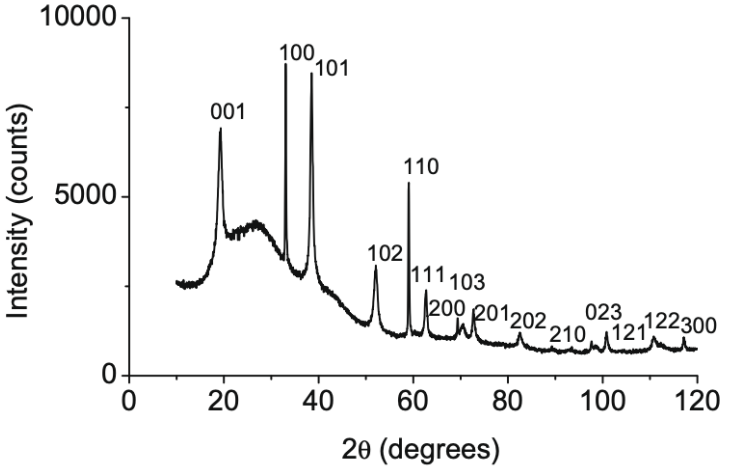


Fig. 1. X-ray diffraction pattern from $Ni(OH)_2$ dispersion c = 4.610(3) Å) with diffraction peaks labeled with hkl indice

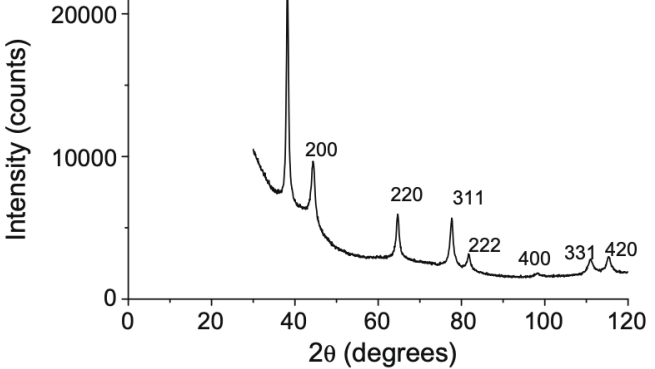


Fig. 2. X-ray diffraction patterns from dispersed Au particles (a = 4.067(3) Å) with diffraction peaks are labeled with hkl indices.

Contents lists available at ScienceDirect



Journal of Colloid and Interface Science

www.elsevier.com/locate/jcis



Use of wide-angle X-ray diffraction to measure shape and size of dispersed colloidal particles

S. Junaid S. Qazi a,*, Adrian R. Rennie , Jeremy K. Cockcroft , Martin Vickers b

Table 1 Results from the pseudo-Voigt function fit to the Ni(OH)₂ sample. 2θ is the peak position for the Cu K α_1 radiation wavelength (0.154056 nm).

hkl	Bragg angle 2θ (°)	Peak width 'β' (°)	Instrument resolution (°)	Corrected β (°)	
001	19.25	1.140	0.121	1.02	
100	33.06	0.197	0.115	0.08	
101	38.52	0.593	0.114	0.48	
102	52.06	0.876	0.117	0.76	
110	59.05	0.248	0.120	0.13	
111	62.67	0.550	0.122	0.43	

Table 2 Results from the pseudo-Voigt fit to the Au particles. 2θ is the peak position for the Cu K α_1 radiation wavelength (0.154056 nm).

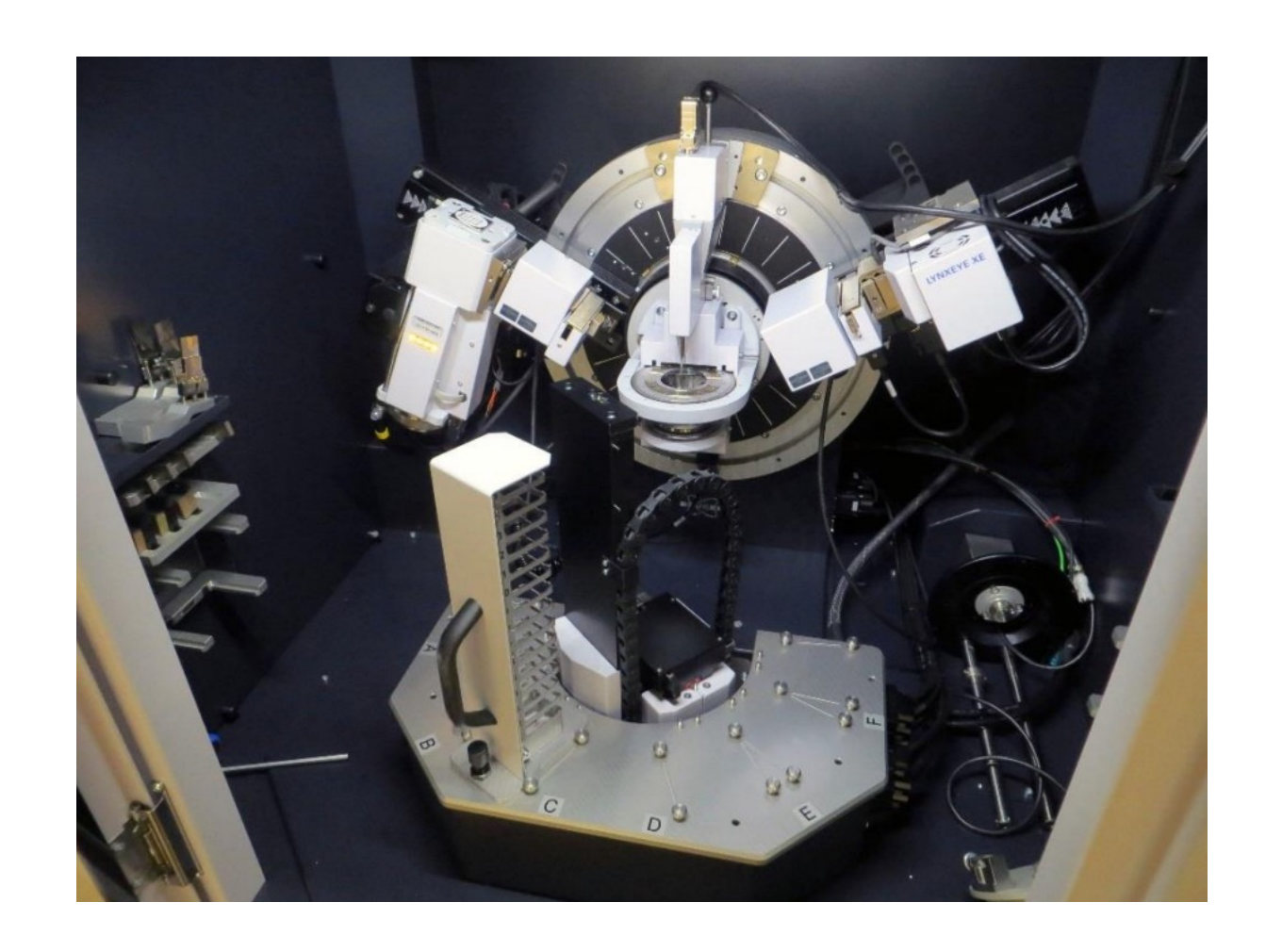
hkl	Bragg angle 2θ (°)	Peak width 'β' (°)	Instrument resolution (°)	Corrected β (°)	
111	38.21	0.580	0.114	0.47	
200	44.34	0.822	0.115	0.71	
220	64.69	0.810	0.123	0.68	
311	77.63	0.905	0.135	0.77	
420	115.34	1.194	0.119	1.07	

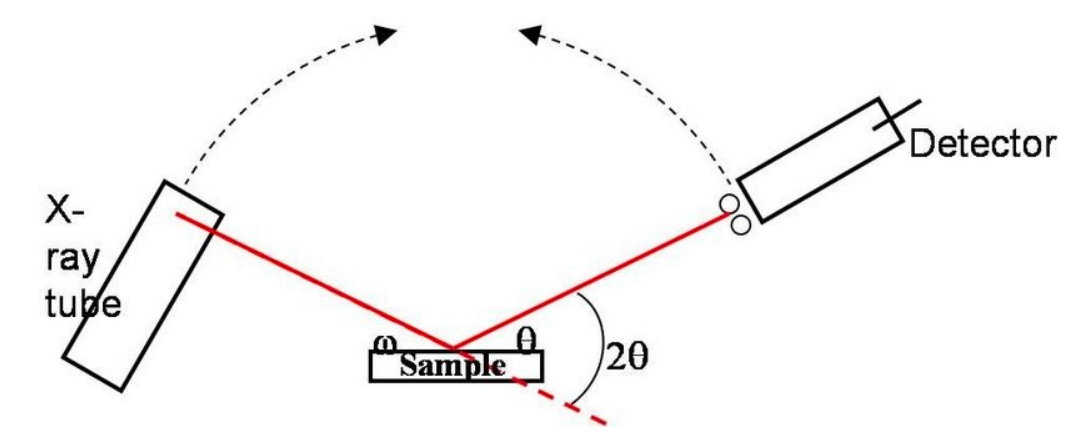
^a Materials Physics, Uppsala University, Ångströmlaboratoriet, Box 530, 75121 Uppsala, Sweden

^b Applied Crystallography Group, Department of Chemistry, University College London, 20 Gordon Street, London WC1H 0AJ, UK

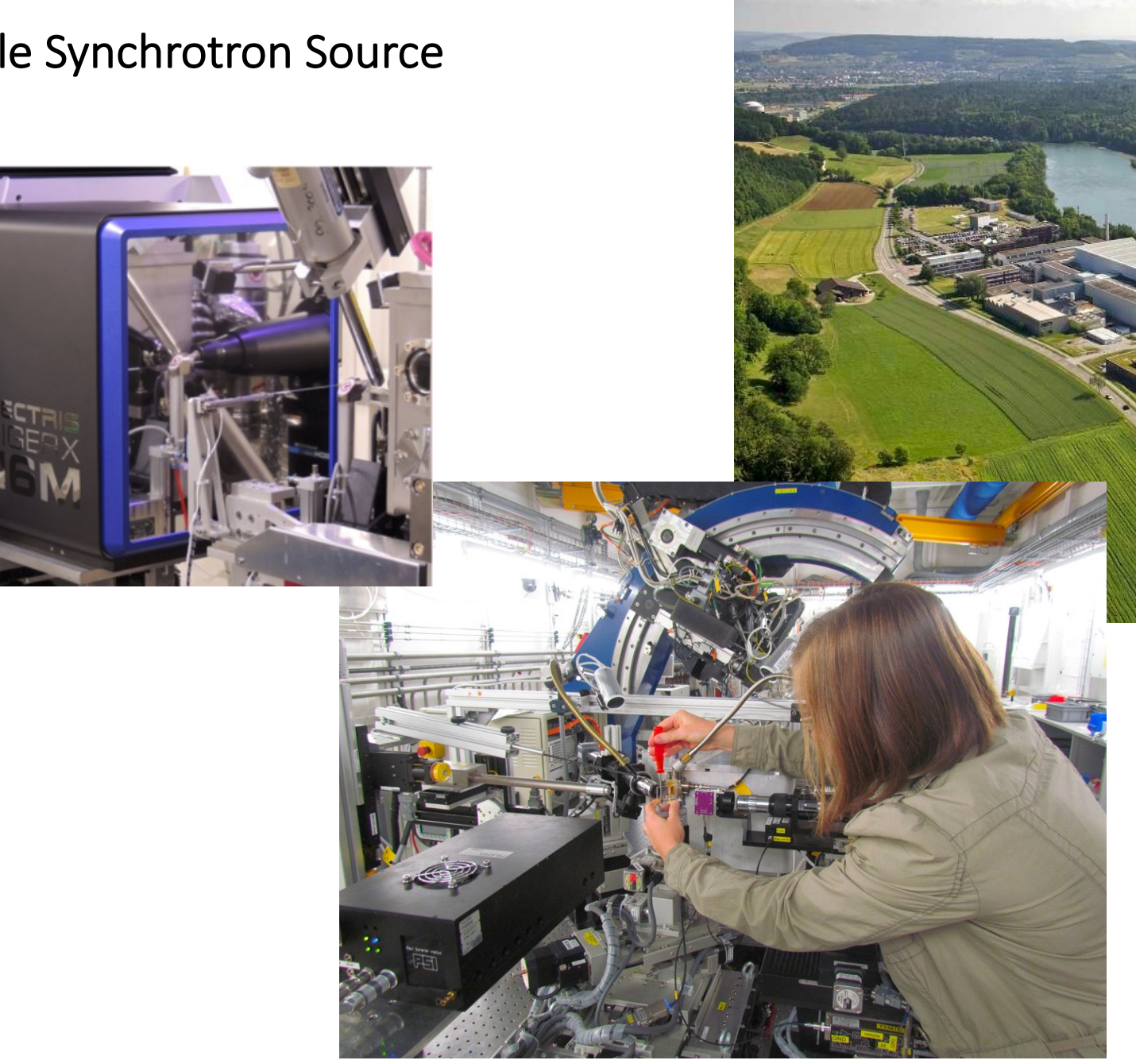
A few examples and case studies

Example: EPFL XRD instrument





Example Synchrotron Source



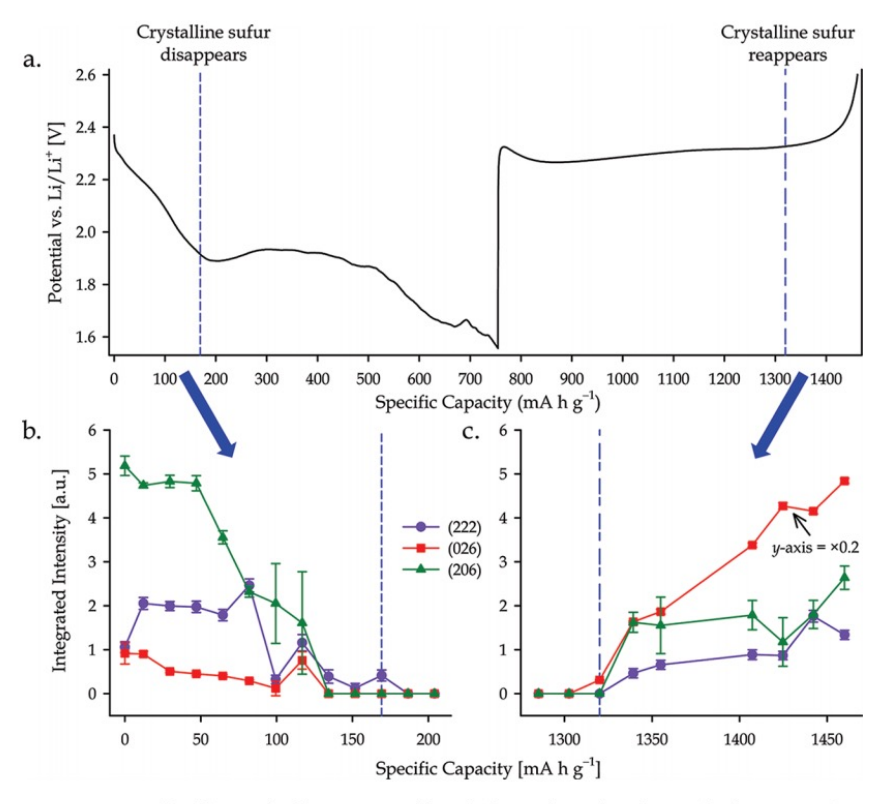
Example: In-operando battery research



In Operando X-ray Diffraction and Transmission X-ray Microscopy of Lithium Sulfur Batteries

Johanna Nelson, $^{\dagger,\pm,\perp}$ Sumohan Misra, $^{\dagger,\perp}$ Yuan Yang, $^{\S,\perp}$ Ariel Jackson, § Yijin Liu, † Hailiang Wang, $^{\parallel}$ Hongjie Dai, $^{\parallel}$ Joy C. Andrews, † Yi Cui, $^{*,\pm,\$}$ and Michael F. Toney $^{*,\dagger,\pm}$

[§]Department of Materials Science and Engineering, and □Department of Chemistry, Stanford University, Stanford, California 94305, United States



Article

pubs.acs.org/JACS

Figure 3. Integrated diffraction intensities of sulfur peaks for a Li–S cell cycled at C/8 and with a cathode prepared as a sulfur/Super P composite: (a) electrochemical plot showing the first cycle of the Li–S cell; (b and c) integrated intensity plots for (222), (026) and (206) Bragg peaks, which show the disappearance of crystalline sulfur by the end of the first discharge plateau and its reappearance by the end of the charge cycle. The blue arrows indicate the specific capacity regions over which the integrated intensities are plotted. The dashed lines emphasize where sulfur peaks disappear and reappear. The total discharge capacity is 755 mA h g⁻¹, and the total charge capacity is 707 mA h g⁻¹. Error bars on the integrated intensities were determined using Levenberg–Marquardt minimization.

37

[†]Stanford Synchrotron Radiation Lightsource, and [‡]Stanford Institute for Materials and Energy Science, SLAC National Accelerator Laboratory, 2575 Sand Hill Road, Menlo Park, California 94025, United States

Example: In operando – laser printing PSI

ARTICLE IN PRESS

Materials Today • Volume xxx. Number xx • xxxx 2019

RESEARCH



Operando X-ray diffraction during laser 3D printing

Samy Hocine ^{1,2}, Helena Van Swygenhoven ^{1,2,*}, Steven Van Petegem ¹, Cynthia Sin Ting Chang ¹, Tuerdi Maimaitiyili ¹, Gemma Tinti ³, Dario Ferreira Sanchez ⁴, Daniel Grolimund ⁴, Nicola Casati ⁵



Materials Today ● Volume xxx, Number xx ● xxxx 2019

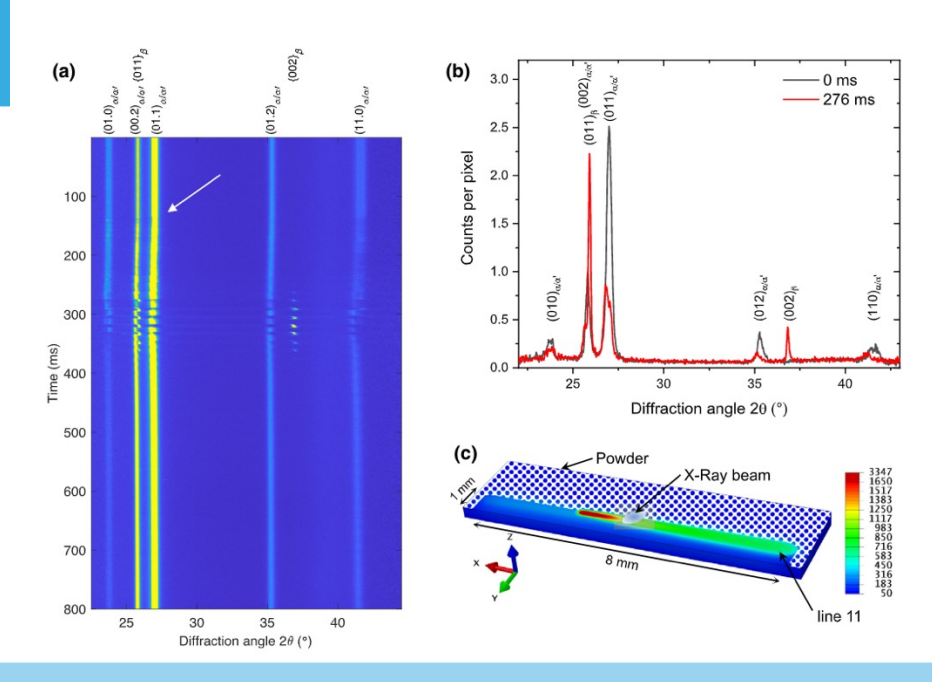


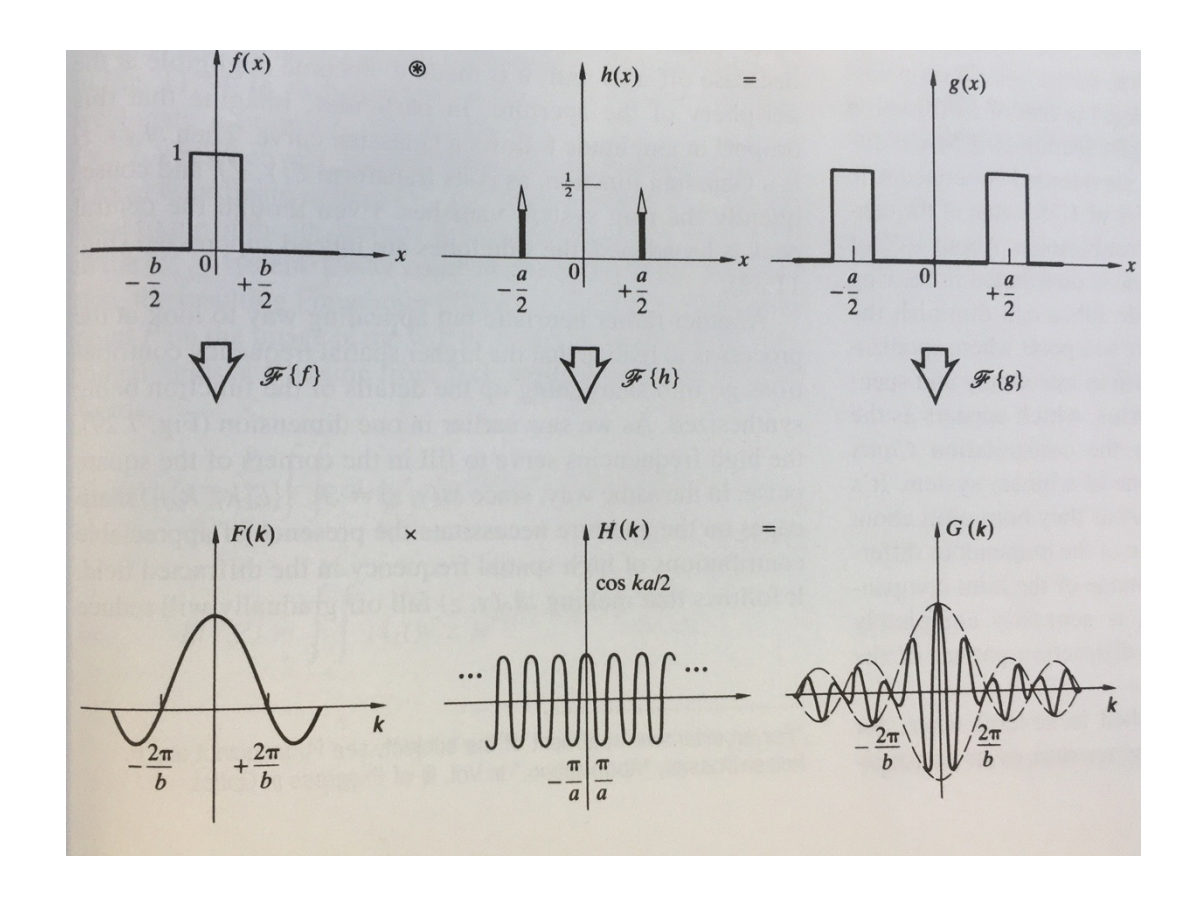
FIGURE 3

(a) Phase evolution during printing of a single layer, shown as an intensity vs. diffraction angle and time by stacking 16,000 individual diffraction patterns. The white arrow indicates the start of the printing process, (b) diffraction patterns recorded prior to printing and during printing of the 11th line at t = 276 ms, (c) schematic representation of the relative position of laser, X-ray beam and HAZ at t = 276 ms. (Temperature scale in degree Celsius).

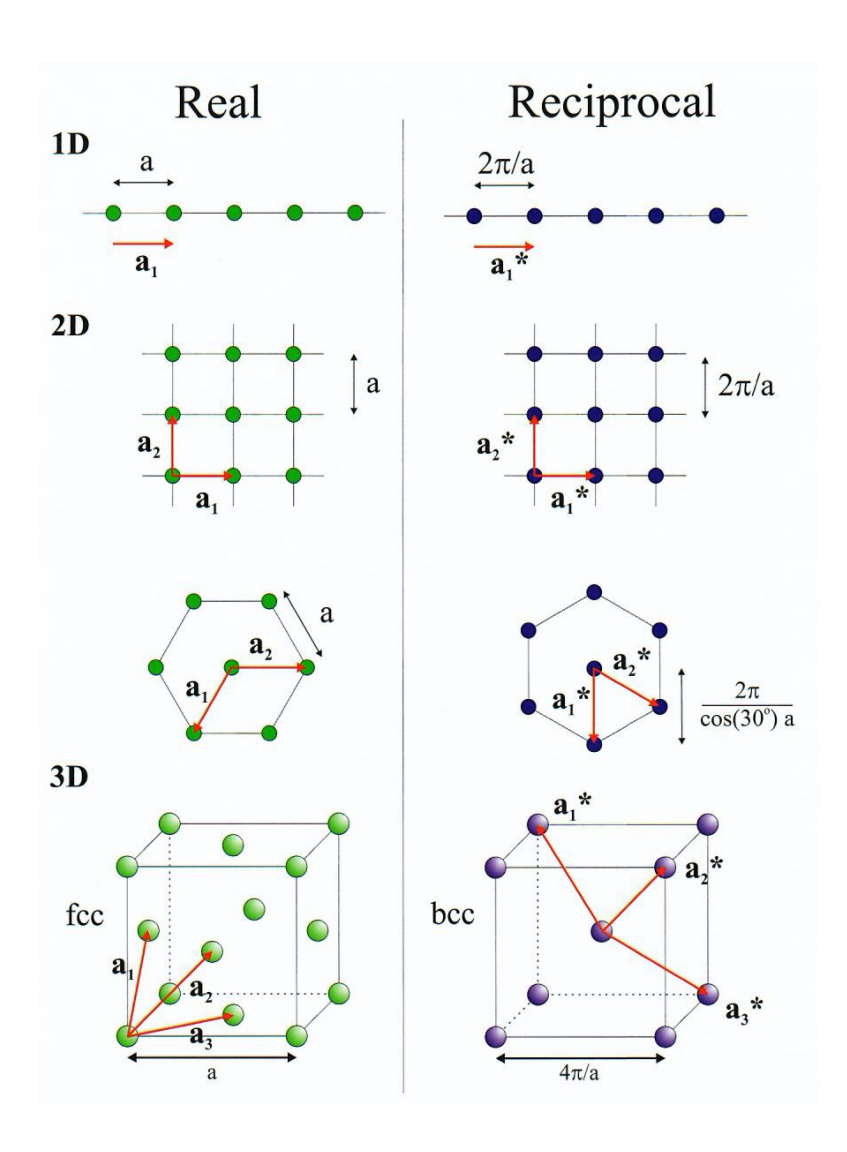
Outlook

Diffraction as Fourier Transform
Reciprocal Lattice
Bragg and Laue Diffraction
Structure Factor
Detailed Electronic Structure Maps

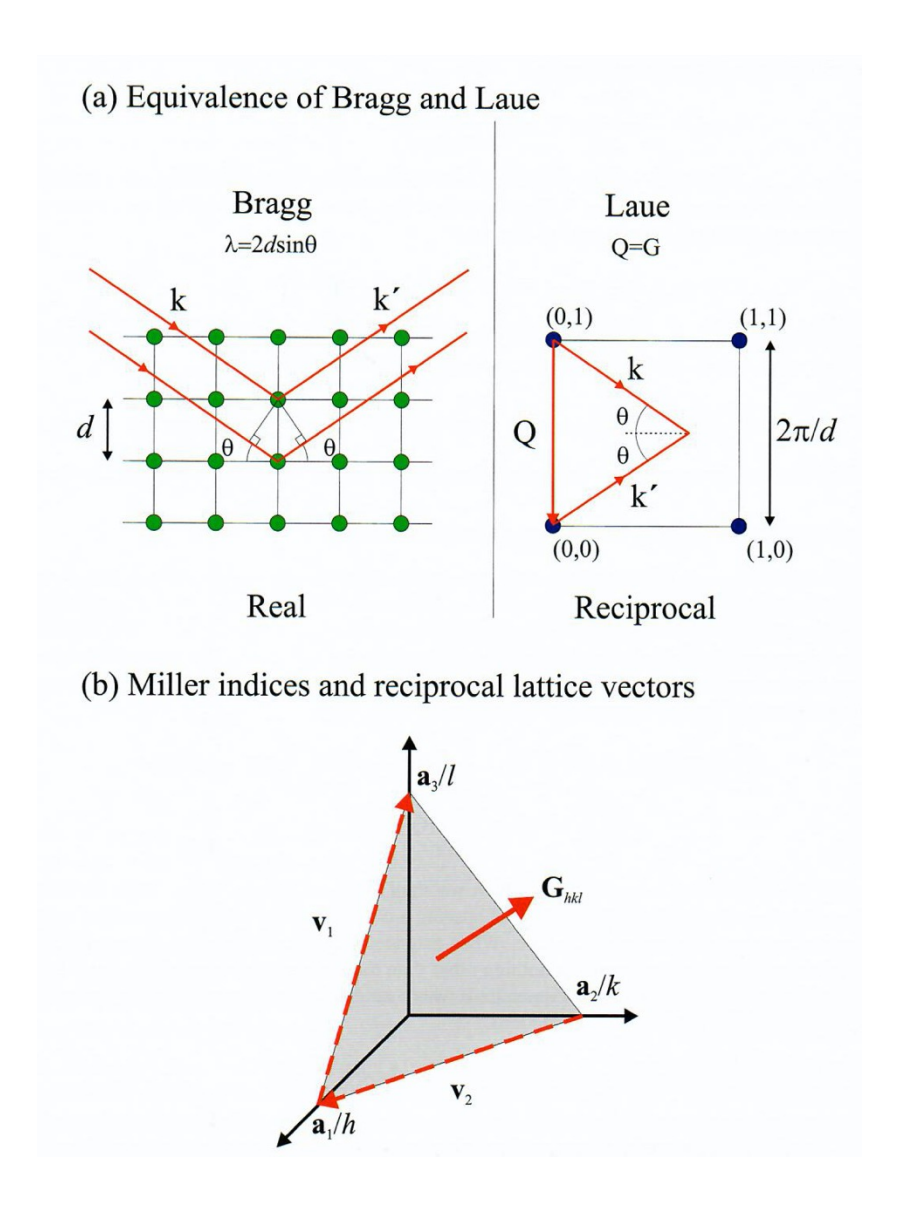
Diffraction as Fourier transform:



For each lattice a reciprocal lattice can be defined



Bargg and Laue conditions



The Nobel Prize in Physics 1914

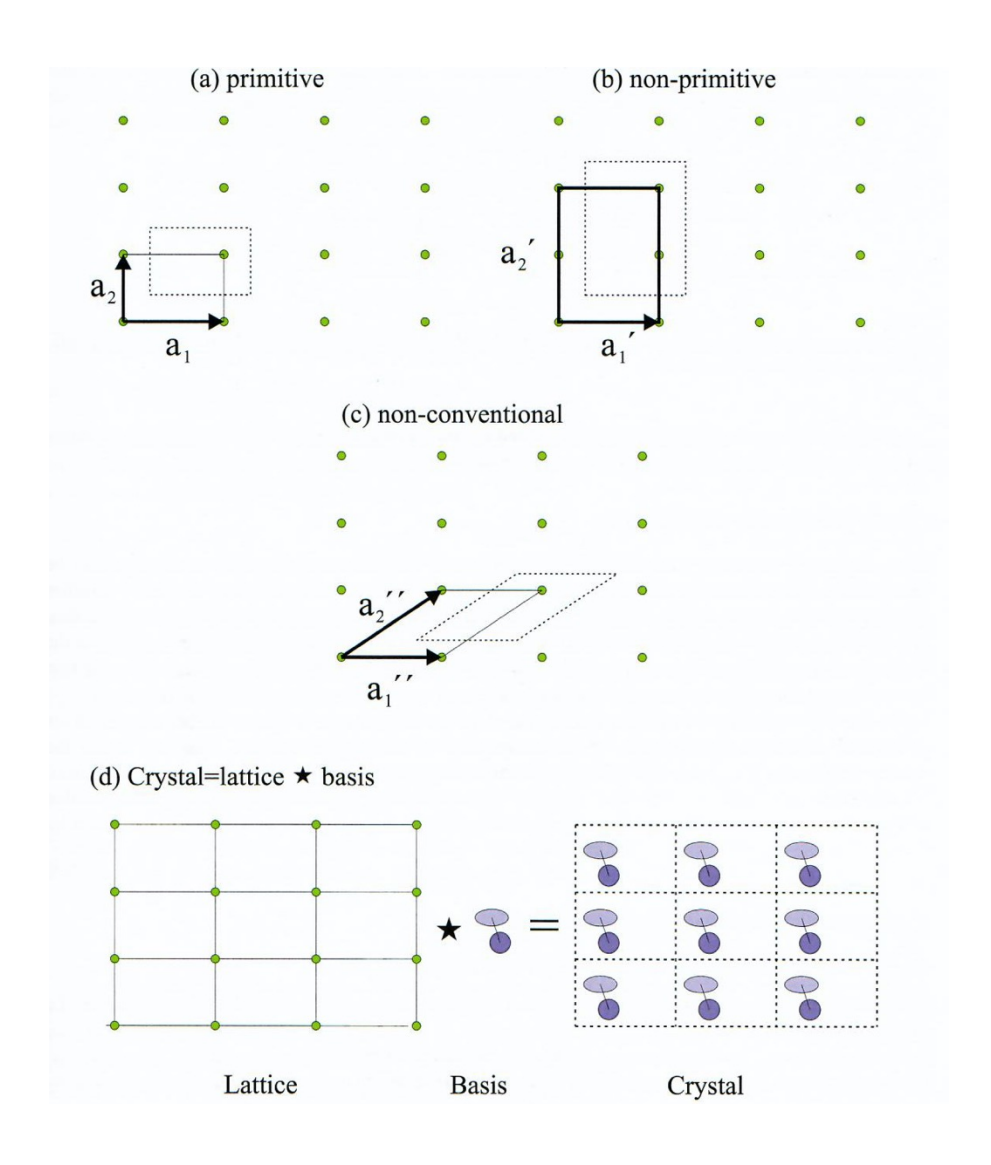


Photo from the Nobel Foundationarchive.

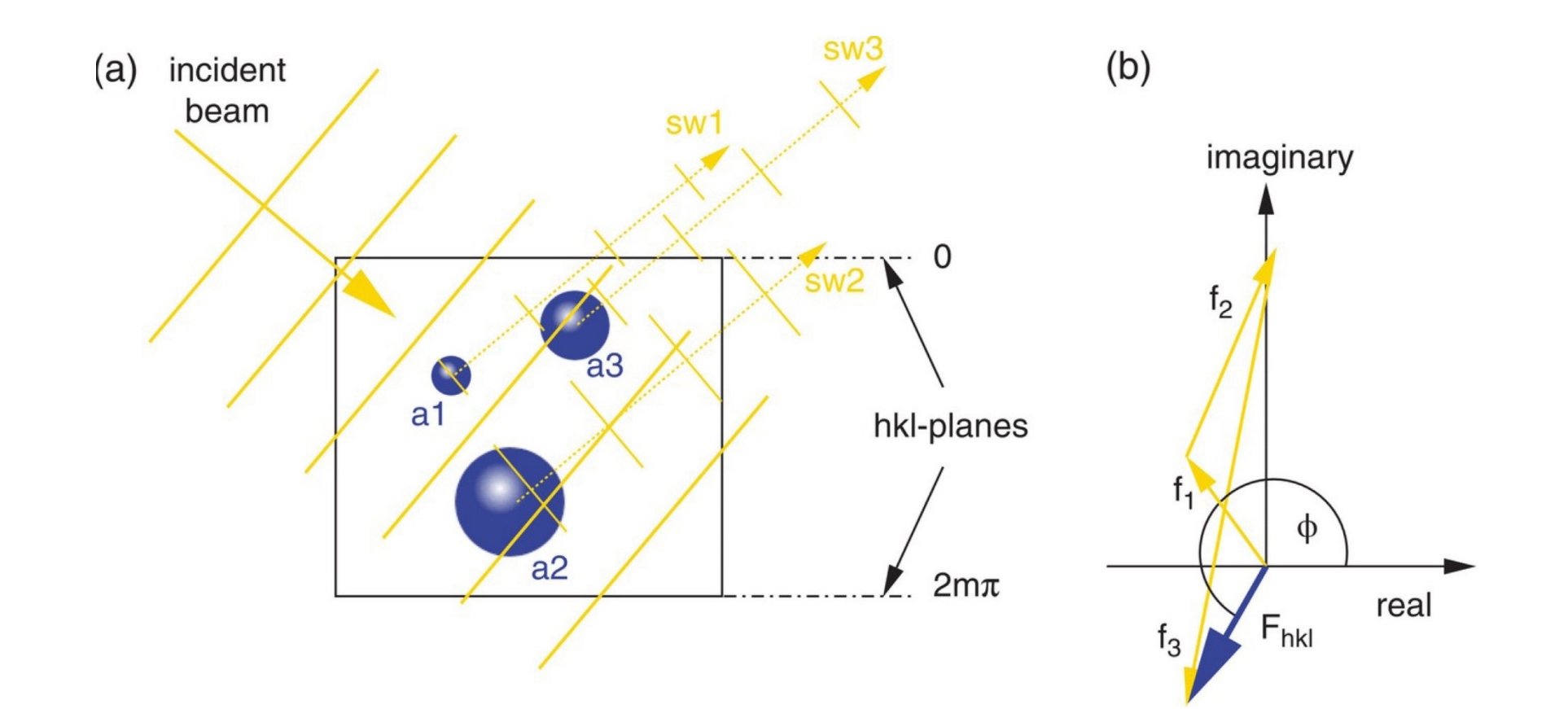
Max von Laue

Prize share: 1/1

A crystal is defined by ist lattice and basis



The structure factor



The end